POSCO Lectures: The Bainite Reaction

H. K. D. H. Bhadeshia, GIFT, POSTECH

1 Introduction

Examination of a time–temperature–transformation (TTT) diagram for an eutectoid carbon steel (Fig. 1), bearing in mind the fact that the pearlite reaction is essentially a high temperature one occurring between $550°$C and $720°$C and that the formation of the martensite is a low-temperature reaction, reveals that there is a wide range of temperature $\sim$250–550°C within which neither of these phases forms. This is the region in which fine aggregates of ferrite plates (or laths) and cementite particles are formed. The generic terms for these intermediate structures is *bainite*, after Edgar Bain who with Davenport first found these structures during their pioneering systematic studies of the isothermal decomposition of austenite. Bainite also occurs during athermal treatments at cooling rates too fast for pearlite to form, yet not rapid enough to produce martensite.

The nature of bainite changes as the transformation temperature is lowered. Two main forms can be identified: *upper* and *lower* bainite.

2 Upper Bainite

The microstructure of upper bainite consists of fine plates of ferrite, each of which is about $0.2\,\mu$m thick and about $10\,\mu$m long. The plates grow in clusters called sheaves. Within each sheaf the plates are parallel and of identical crystallographic orientation, each with a well-defined crystallographic habit. The individual plates in a sheaf are often called the 'sub-units' of bainite. They are usually separated by low-misorientation boundaries or by cementite particles (Fig. 2).

Upper bainite evolves in distinct stages beginning with the nucleation of ferrite plates at the austenite grain boundaries. The growth of each plate is accompanied by a change in the shape of the transformed region (Fig. 3), a change which can be described precisely as an invariant-plane strain (IPS) with a large shear component, virtually identical to that observed during martensitic transformation [1]. However, bainite grows at relatively high temperatures when compared with martensite. The large strains associated with the shape change cannot be sustained by the austenite, the strength of which decreases as the temperature rises. These strains are relaxed by the plastic deformation of the adjacent austenite. The local increase in dislocation density caused by the yielding of the austenite blocks the further movement of the glissile transformation interface (Fig. 3). This localized plastic deformation therefore halts the growth of the ferrite plate so that each sub-unit only achieves a limited size which is much less than the size of an austenite grain.

As with martensite, the shape change implies that the mechanism of growth of bainitic ferrite is displacive. It is the minimization of the strain energy associated with the displacements that ensures that bainite grows in the form of thin plates. Since the crystal structure of bainite is generated by a coordinated movement of atoms, it follows that there must exist an orientation relationship between the austenite and the bainite. This relationship is found experimentally to be of the type where a pair of the most densely packed planes of the two lattices are approximately parallel, as are a corresponding pair of close-packed directions within those planes.
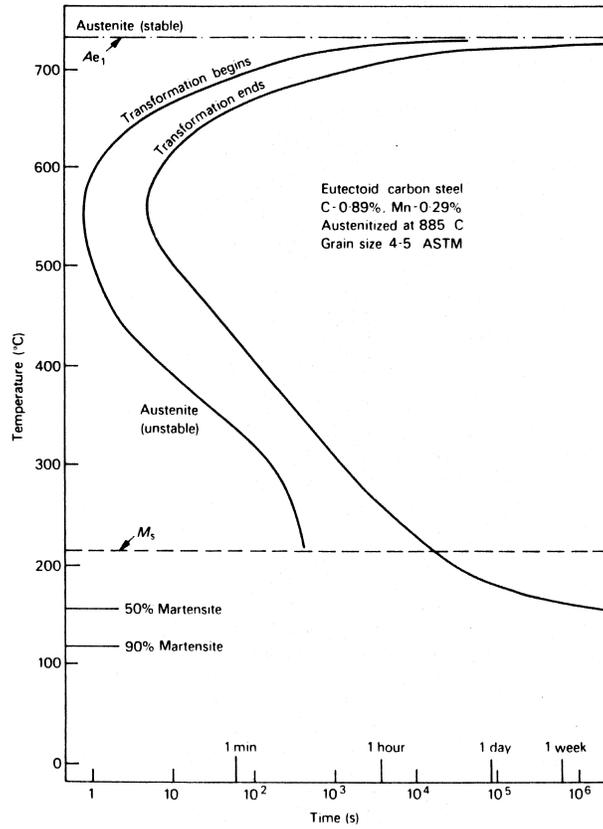
Figure 1: TTT diagram for a 0.89 wt% carbon steel.
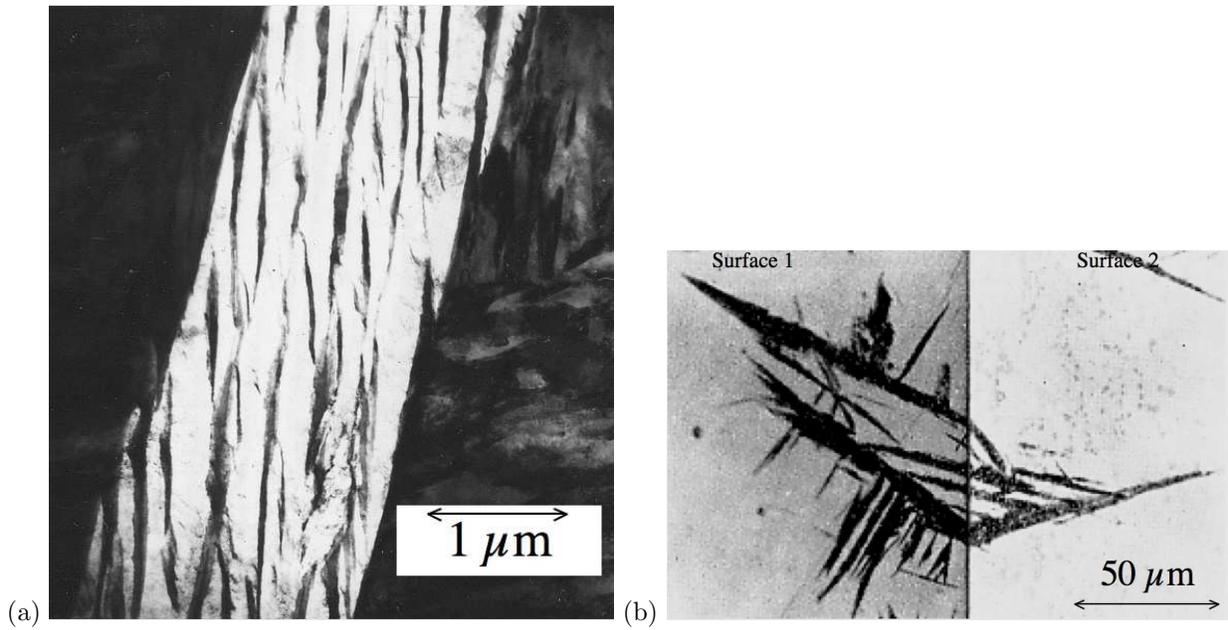
Figure 2: (a) Upper bainite. (b) Two–surface optical micrograph.

(a)

(b)
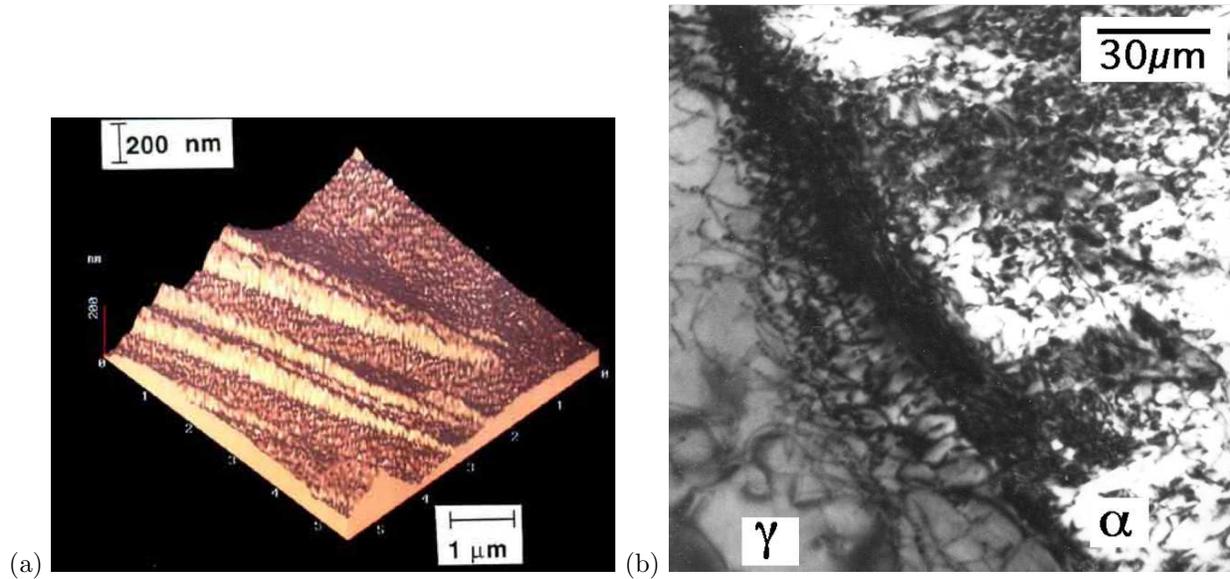
Figure 3: (a) Surface relief caused by the formation of bainite in a sample which was first polished and then transformed. (b) Intense dislocation debris at a bainite/austenite interface.

This is loosely described by a Kurdjumov–Sachs type orientation relationship.

Bainite forms on particular crystallographic planes, but the indices of the habit plane show considerable scatter (Fig. 4). This is because most of the measurements are made using light microscopy, in which case the habit plane determined is not that of an individual sub-unit. It corresponds instead to some average value depending on the number, size and distribution of sub-units within the sheaf. All of these factors can vary with the transformation temperature, time and chemical composition.

Fe–0.92C–0.22Mn–0.03Si Wt%
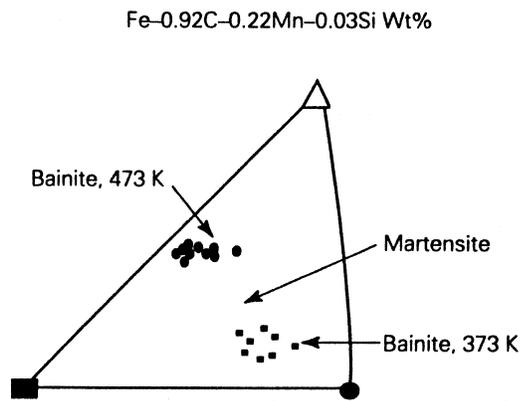
Figure 4: Stereographic triangle showing the habit plane of bainite compared with that of martensite in the same steel [2].

It was emphasized earlier that upper bainite forms in two distinct stages, the first involving the formation of bainitic ferrite which has a very low solubility for carbon (<0.02 wt%). The growth of the ferrite therefore enriches the remaining austenite in carbon. Eventually, cementite precipitates from the residual austenite layers in between the ferrite sub-units. The amount of cementite depends on the carbon concentration of the alloy. High concentrations lead to microstructures in which the ferrite platelets are separated by continuous layers of cementite. Small, discrete particles of cementite form when the alloy carbon concentration is low.

The cementite particles have a 'Pitsch' orientation relationship with the austenite from which they precipi-

tate:

$$[\ 0\quad 0\quad 1\ ]_{\text{Fe}_3\text{C}} \,\|\, [\ \bar{2}\quad 2\quad 5\ ]_\gamma,$$
$$[\ 1\quad 0\quad 0\ ]_{\text{Fe}_3\text{C}} \,\|\, [\ 5\quad \bar{5}\quad 4\ ]_\gamma,$$
$$[\ 0\quad 1\quad 0\ ]_{\text{Fe}_3\text{C}} \,\|\, [\ \bar{1}\quad \bar{1}\quad 0\ ]_\gamma.$$

Many variants of carbide may precipitate from the austenite, each particle being indirectly related to the ferrite via the ferrite/austenite orientation relationship.

If sufficient quantities of alloying elements (such as Si or Al) which retard the formation of cementite are added to the steel, then it is possible to suppress the formation of cementite altogether. An upper bainite microstructure consisting of just bainitic ferrite and carbon-enriched retained austenite is obtained instead (Fig. 5). The microstructure may also contain martensite if the residual austenite decomposes on cooling to ambient temperature.
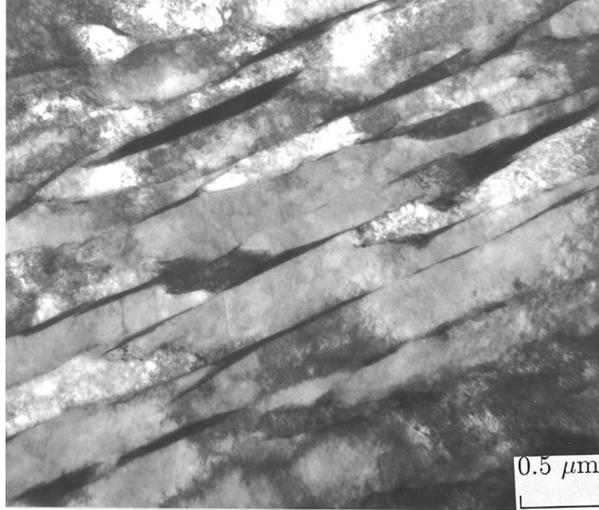
Figure 5: Upper bainite with retained austenite between platelets.

3 Lower Bainite

Lower bainite has a microstructure and crystallographic features which are very similar to those of upper bainite. The major distinction is that cementite particles also precipitate inside the plates of ferrite (Fig. 6). There are, therefore, two kinds of cementite precipitates: those which grow from the carbon-enriched austenite which separates the platelets of bainitic ferrite, and others which appear to precipitate from supersaturated ferrite. These latter particles exhibit the 'tempering' orientation relationship which is found when carbides precipitate during the heat treatment of martensite, often described as the Bagaryatski orientation relationship:

$$[\ 0\quad 0\quad 1\ ]_{\text{Fe}_3\text{C}} \,\|\, [\ \bar{1}\quad 0\quad 1\ ]_\alpha,$$
$$[\ 1\quad 0\quad 0\ ]_{\text{Fe}_3\text{C}} \,\|\, [\ 1\quad 1\quad 1\ ]_\alpha,$$
$$[\ 0\quad 1\quad 0\ ]_{\text{Fe}_3\text{C}} \,\|\, [\ \bar{1}\quad 2\quad \bar{1}\ ]_\alpha.$$

The carbides in the ferrite need not always be cementite. Depending on the chemical composition and the transformation temperature, other transition carbides may precipitate first. For example, in high-carbon steels containing more than about $1\,\text{wt}\%$ silicon (which retards cementite formation), epsilon carbide is commonly observed to precipitate in the bainitic ferrite.
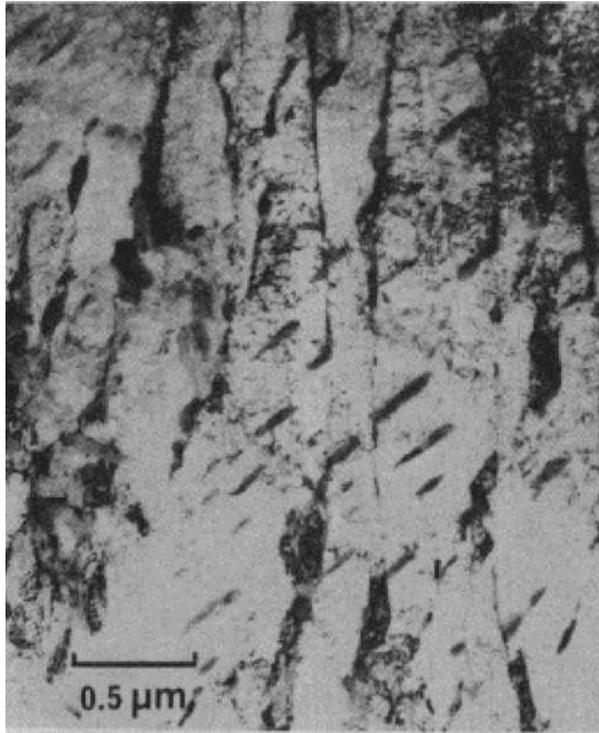
Figure 6: Lower bainite.

In contrast to tempered martensite, the cementite particles in lower bainite frequently precipitate in just one variant of the orientation relationship (Fig. 6), such that they form parallel arrays at about 60° to the axis of the bainite plate. In tempered martensite, the carbides tend to precipitate in Widmanstätten arrays.

However, these general observations are not always true. Widmanstätten arrays of cementite are also found in lower bainite when the latter forms in high-carbon steels or when the transformation occurs at low temperatures. Similarly, martensite in low-carbon steels exhibits only a single variant of carbide on tempering. This is because the carbide precipitation is influenced by the stresses associated with the displacive growth of lower bainite or martensite – those variants of cementite which best comply with the stress are dominant. If the driving force for precipitation is large (i.e. the carbon concentration inherited by the bainite is large) then multiple variants including those which do not comply with the stress are able to precipitate.

The carbides in the lower bainite are extremely fine, just a few nanometres thick and about 500 nm long. Because they precipitate within the ferrite, a smaller amount of carbon is partitioned into the residual austenite. This in turn means that fewer and finer cementite particles precipitate between the ferrite plates, when compared with an upper bainitic microstructure. An important consequence is that lower bainite is usually found to be much tougher than upper bainite, in spite of the fact that it also tends to be stronger. The coarse cementite particles in upper bainite are notorious in their ability to nucleate cleavage cracks and voids.

4   The Shape Change

The IPS surface relief caused by the growth of bainitic ferrite has a large shear strain component of 0.24 in addition to the volume strain (0.03) on transformation. There is, therefore, a coordinated movement of atoms as the transformation occurs. Consistent with this, the iron and substitutional solutes such as

Mn, Si, Ni, Mo and Cr, have been demonstrated using high-resolution techniques to be frozen into position during transformation (Fig. 7). The change in crystal structure is therefore achieved by a deformation of the austenite crystal. If the strain is elastically accommodated, then the strain energy of bainitic ferrite amounts to about $400 \, \mathrm{J \, mol^{-1}}$. Some of the strain can be relaxed by plastic deformation in the adjacent austenite.
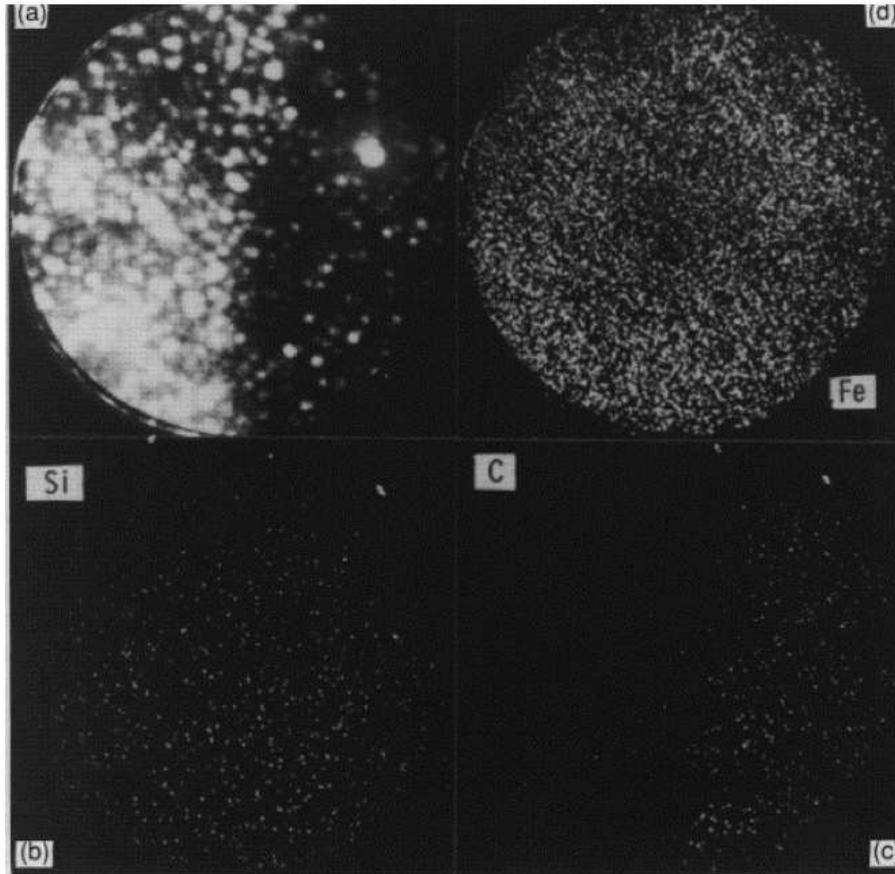
Figure 7: Imaging atom-probe micrographs, taken across an austenite–bainitic ferrite interface in a Fe–C–Si–Mn alloy. Substitutional atoms clearly do not diffuse during transformation. (a) Field ion image; each dot corresponds to an atom. The interface is vertical in the image, the austenite located on the right-hand side. (b) Fe atom map. (c) Corresponding Si atom map, showing a uniform distribution. (d) C atom map [3].

The movement of interstitial atoms during the change in crystal structure does not influence the development of surface relief. Conversely, the observation of relief cannot yield information about whether or not carbon diffuses during transformation.

5   Carbon in Bainite

It is simple to establish that martensitic transformation is diffusionless, by measuring the local compositions before and after transformation. Bainite forms at somewhat higher temperatures where the carbon can escape out of the plate within a fraction of a second. Its original composition cannot therefore be measured directly.

There are three possibilities. The carbon may partition during growth so that the ferrite may never contain

any excess carbon. The growth may on the other hand be diffusionless with carbon being trapped by the advancing interface. Finally, there is an intermediate case in which some carbon may diffuse with the remainder being trapped to leave the ferrite partially supersaturated. It is therefore much more difficult to determine the precise role of carbon during the growth of bainitic ferrite than in martensite.

Diffusionless growth requires that transformation occurs at a temperature below T_0, when the free energy of bainite becomes less than that of austenite of the same composition. A locus of the T_0 temperature of the function of the carbon concentration is called the T_0 curve, an example of which is plotted on the Fe–C phase diagram in Fig. 8. Growth without diffusion can only occur if the carbon concentration of the austenite lies to the left of the T_0 curve.
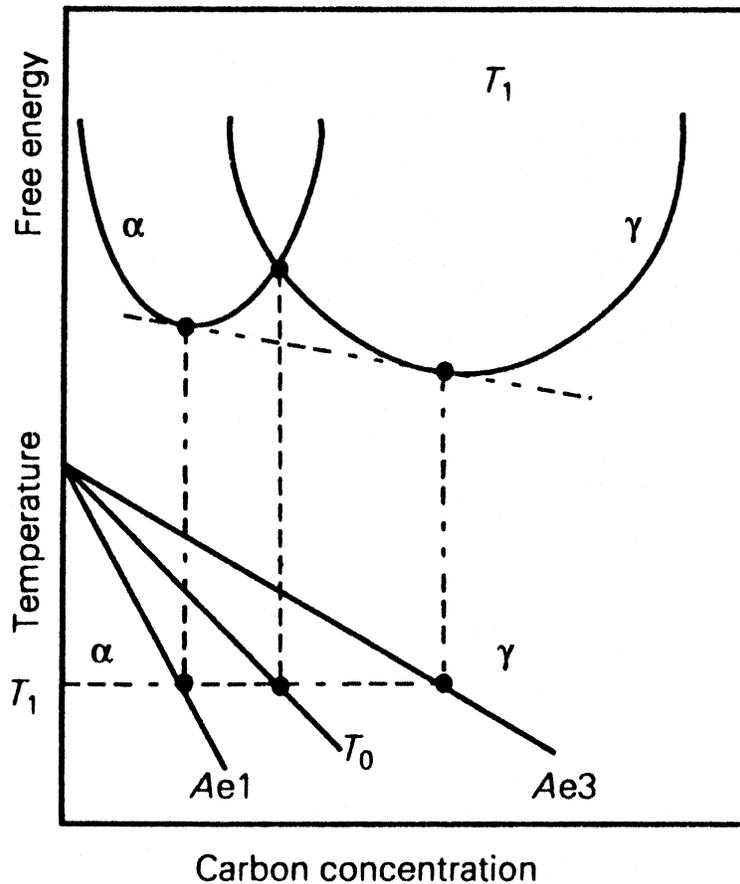
Figure 8: Schematic illustration of the origin of the T_0 construction on the Fe–C phase diagram. Austenite with a carbon concentration to the left of the T_0 boundary can in principle transform without any diffusion. Diffusionless transformation is thermodynamically impossible if the carbon concentration of the austenite exceeds the T_0 curve.

Suppose that the plate of bainite forms without diffusion, but that any excess carbon is soon afterwards rejected into the residual austenite. The next plate of bainite then has to grow from carbon-enriched austenite (Fig. 9). This process must cease when the austenite carbon concentration reaches the T_0 curve. The reaction is said to be incomplete, since the austenite has not achieved its equilibrium composition (given by the Ae_3 curve) at the point the reaction stops. If on the other hand, the ferrite grows with an equilibrium carbon concentration then the transformation should cease when the austenite carbon concentration reaches the Ae_3 curve.

It is found experimentally that the transformation to bainite does indeed stop at the T_0 boundary (Fig. 9b).
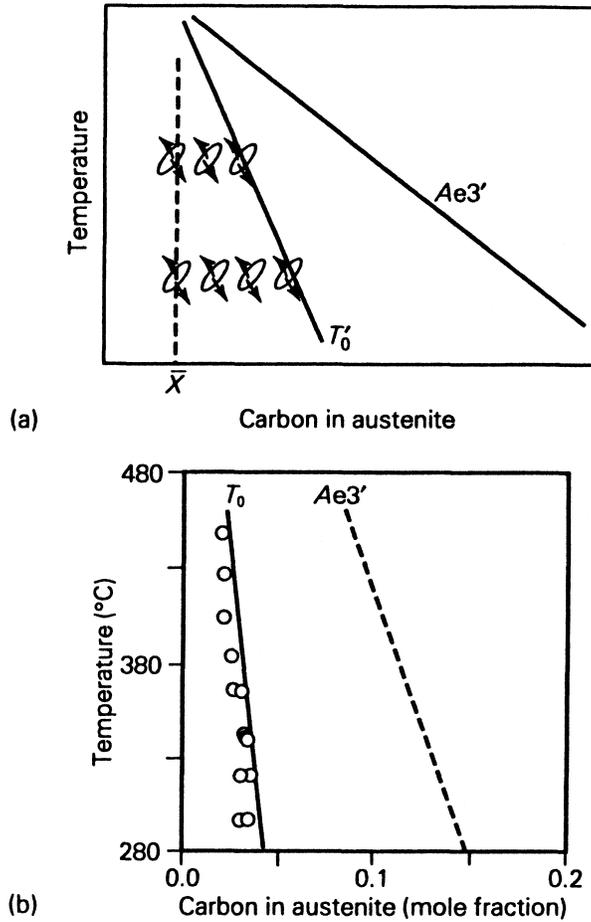
Figure 9: (a) Illustration of the incomplete-reaction phenomenon. During isothermal transformation, a plate of bainite grows without diffusion, then partitions its excess carbon into the residual austenite. The next plate therefore has to grow from carbon-enriched austenite. This process continues until diffusionless transformation becomes impossible when the austenite composition eventually reaches the T_0 boundary. (b) Experimental data showing that the growth of bainite stops when the austenite carbon concentration reaches the T_0 curve (Fe–0.43C–3Mn–2.12Si wt% alloy).

The balance of the evidence is that the growth of bainite below the B_s temperature involves the successive nucleation and martensitic growth of sub-units, followed in upper bainite by the diffusion of carbon into the surrounding austenite. The possibility that a small fraction of the carbon is nevertheless partitioned during growth cannot entirely be ruled out, but there is little doubt that the bainite is at first substantially supersaturated with carbon.

These conclusions are not significantly modified when the strain energy of transformation is included in the analysis.

There are two important features of bainite which can be shown by a variety of techniques, e.g. dilatometry, electrical resistivity, magnetic measurements and by metallography. Firstly, there is a well-defined temperature B_s above which no bainite will form, which has been confirmed for a wide range of alloy steels. The amount of bainite that forms increases as the transformation temperature is reduced below the B_s temperature. The fraction increases during isothermal transformation as a sigmoidal function of time, reaching an asymptotic limit which does not change on prolonged heat treatment even when substantial quantities of austenite remain untransformed. Transformation in fact ceases before the austenite achieves its equilibrium

8

composition, so that the effect is dubbed the 'incomplete-reaction phenomenon'. These observations are understood when it is realized that growth must cease if the carbon concentration in the austenite reaches the T_0 curve of the phase diagram.

Since this condition is met at ever-increasing carbon concentrations when the transformation temperature is reduced, more bainite can form with greater undercoolings below B_s. But the T_0 restriction means that equilibrium, when the austenite has a composition given by the Ae_3 phase boundary, can never be reached, as observed experimentally. A bainite-finish temperature B_F is sometimes defined, but this clearly cannot have any fundamental significance.

6 Thermodynamics and Kinetics of Nucleation

6.1 Thermodynamics

There is a change in the chemical composition of the austenite when it partly decomposes into ferrite. In contrast, the formation of a ferrite nucleus hardly affects the composition of the remaining austenite. The calculation of the free energy change for nucleation takes this difference into account. The free energy change for the formation of a mole of ferrite nuclei of composition x^α is given by ΔG_3, Fig. 10a [4, 5].
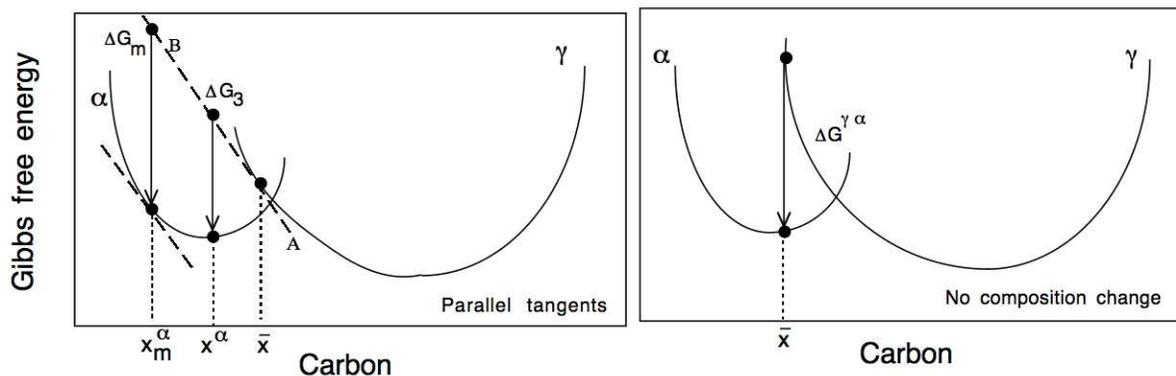
Figure 10: Free energy diagrams illustrating (a) the chemical free energy changes during the nucleation and (b) the growth of bainitic–ferrite from austenite of composition $\overline{x}$.

The greatest reduction in free energy during nucleation is obtained if the composition of the ferrite nucleus is set to a value x_m, given by a tangent to the ferrite free energy curve which is parallel to the tangent to the austenite free energy curve at $\overline{x}$, as shown in Fig. 10a. This maximum possible free energy change for nucleation is designated ΔG_m.

There is simplification when the transformation occurs without composition change (Fig. 10b). The change $\Delta G^{\gamma\alpha}$ is the vertical distance between the austenite and ferrite free energy curves at the composition of interest.

We shall henceforth use ΔG_m for the case where nucleation occurs by a paraequilibrium mechanism and $\Delta G^{\gamma\alpha}$ for cases where there is no change in composition on transformation.

6.2 Transformation–Start Temperature

It is a common observation that the Widmanstätten ferrite–start (W_S) and bainite–start (B_S) temperatures are more sensitive to the steel composition than is the Ae_3 equilibrium–temperature. The influence of solutes

on the nucleation of Widmanstätten ferrite and bainite is more than just thermodynamic, Fig. 11.
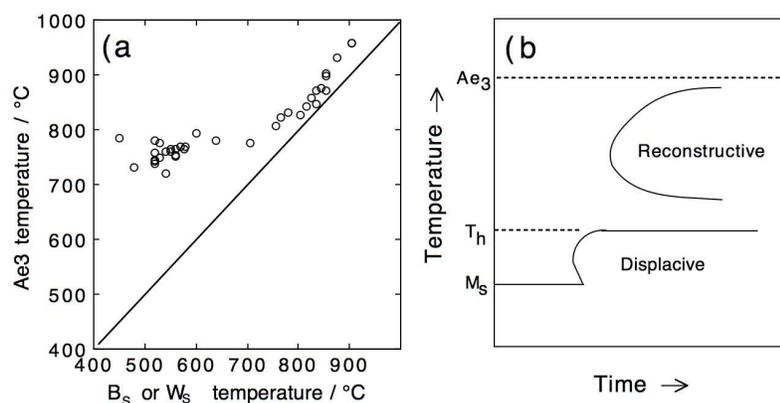
Figure 11: (a) Variation of the Widmanstätten ferrite–start and bainite–start temperatures as a function of the Ae_3 temperature [6]. (b) Schematic TTT diagram illustrating the two C–curves and the T_h temperature, which can be W_S or B_S depending on the prevailing thermodynamic conditions.

Some clues to this behaviour come from studies of time–temperature–transformation diagrams, which consist essentially of two C–curves. The lower C–curve has a characteristic flat top at a temperature T_h, which is the highest temperature at which ferrite can form by displacive transformation, Fig. 11. The transformation product at T_h may be Widmanstätten ferrite or bainite.

The driving force ΔG_m available for nucleation at T_h, is plotted in Fig. 12a, where each point comes from a different steel. The transformation product at T_h can be Widmanstätten ferrite or bainite, but it is found that there is no need to distinguish between these phases for the purposes of nucleation. The same nucleus can develop into either phase depending on the prevailing thermodynamic conditions. The analysis proves that carbon must partition during the nucleation stage to provide the free energy required for nucleation. Diffusionless nucleation is not viable since it would in some cases lead to an increase in the free energy, Fig. 12b.
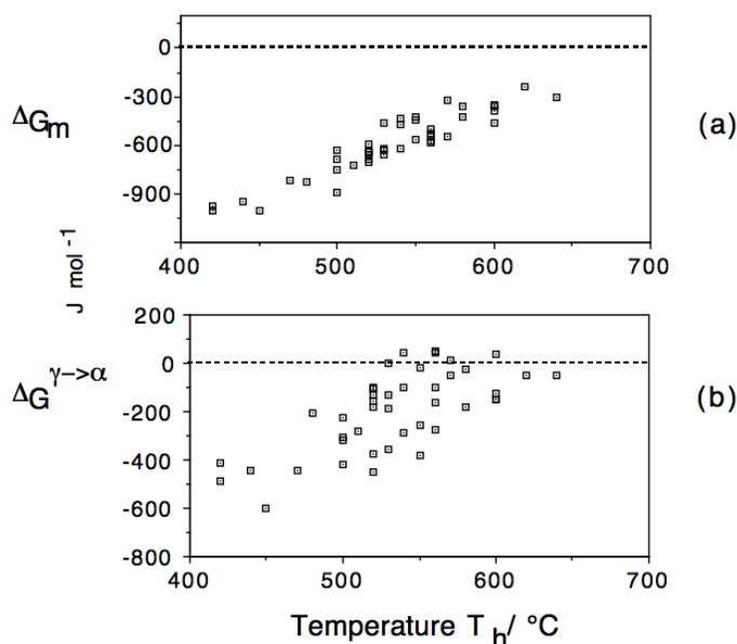
Figure 12: The free energy change necessary in order to obtain a detectable degree of transformation. Each point represents a different steel and there is no distinction made between Widmanstätten ferrite or bainite. (a) Calculated assuming the partitioning of carbon during nucleation. (b) Calculated assuming that there is no change in composition during nucleation. After [4, 5].

The plots in Fig. 12 are generated using data from diverse steels. Fig. 12a represents the free energy change ΔG_m at the temperature T_h where displacive transformation first occurs. The free energy change can be

calculated from readily available thermodynamic data. It follows that Fig. 12a can be used to estimate T_h for any steel. The equation fitted to the data in Fig. 12a is [4, 5, 6]:

$$G_N = C_1(T - 273.18) - C_2 \qquad \text{J\,mol}^{-1} \tag{1}$$

where C_1 and C_2 are fitting constants for the illustrated temperature range. The linear relation between G_N and T is termed a *universal nucleation function*, because it defines the minimum driving force necessary to achieve a perceptible nucleation rate for Widmanstätten ferrite or bainite in any steel.

6.3   Evolution of the Nucleus

The nucleus is identical for Widmanstätten ferrite and for bainite; the transformations are distinguished by their growth mechanisms. But what determines whether the nucleus evolves into bainite or Widmanstätten ferrite?

The answer is straightforward. If diffusionless growth cannot be sustained at T_h then the nucleus develops into Widmanstätten ferrite so that T_h is identified with W_S. A larger undercooling is necessary before bainite can be stimulated. If, however, the driving force at T_h is sufficient to account for diffusionless growth, then $T_h = B_S$ and Widmanstätten ferrite does not form at all.

It follows that Widmanstätten ferrite forms below the Ae_3 temperature when:

$$\Delta G^{\gamma \rightarrow \gamma' + \alpha} < -G_{SW} \qquad \text{and} \qquad \Delta G_m < G_N \tag{2}$$

where G_{SW} is the stored energy of Widmanstätten ferrite (about 50 J\,mol^{-1}). $\Delta G^{\gamma \rightarrow \gamma' + \alpha}$ is the free energy change associated with the paraequilibrium growth of Widmanstätten ferrite [7]. The first of these conditions ensures that the chemical free energy change exceeds the stored energy of the Widmanstätten ferrite, and the second that there is a detectable nucleation rate.

Bainite is expected below the T_0' temperature when:

$$\Delta G^{\gamma \alpha} < -G_{SB} \qquad \text{and} \qquad \Delta G_m < G_N \tag{3}$$

where G_{SB} is the stored energy of bainite (about 400 J\,mol^{-1}). The universal function, when used with these conditions, allows the calculation of the Widmanstätten ferrite–start and bainite–start temperatures from a knowledge of thermodynamics alone.

In this scheme, carbon is partitioned during nucleation but in the case of bainite, not during growth which is diffusionless. There is no inconsistency in this concept since a greater fraction of the free energy becomes available as the particle surface to volume ratio, and hence the influence of interfacial energy, decreases.

6.4   Mechanism of Nucleation

The universal function G_N was originally derived by fitting to experimental data over the temperature range 400–650°C [4, 6] and has been demonstrated more recently for high–carbon steels [8]. It is nevertheless empirical and requires some justification for the linear dependence of G_N on T_h (Fig. 12) before it can be extrapolated to explore low transformation temperatures and address the question about the minimum temperature at which bainite can be obtained.

Classical nucleation theory involving hetrophase fluctuations is not appropriate for bainite [5] given that thermal activation is in short supply. Furthermore, it leads to a relationship between the chemical driving force ΔG_{CHEM} and the activation energy G^* for nucleation as

$$G* \propto \Delta G_{CHEM}^{-2} \tag{4}$$

which cannot explain the proportionality between G_N and T_h [5].

11

One mechanism in which the barrier to nucleation becomes sufficiently small involves the spontaneous dissociation of specific dislocation defects in the parent phase [9, 10]. The dislocations are glissile so the mechanism does not require diffusion. The only barrier is the resistance to the glide of the dislocations. The nucleation event cannot occur until the undercooling is sufficient to support the faulting and strains associated with the dissociation process that leads to the creation of the new crystal structure.

The free energy per unit area of fault plane is:

$$G_F = n_P \rho_A (\Delta G_{CHEM} + G_{STRAIN}) + 2\sigma_{\alpha\gamma}\{n_P\} \tag{5}$$

where n_P is the number of close–packed planes participating in the faulting process, ρ_A is the spacing of the close–packed planes on which the faulting is assumed to occur. The fault energy can become negative when the austenite becomes metastable.

For a fault bounded by an array of n_P dislocations each with a Burgers vector of magnitude b, the force required to move a unit length of dislocation array is $n_P \tau_o b$. τ_o is the shear resistance of the lattice to the motion of the dislocations. G_F provides the opposing stress via the chemical free energy change ΔG_{CHEM}; the physical origin of this stress is the fault energy which becomes negative so that the partial dislocations bounding the fault are repelled. The defect becomes unstable, *i.e.,* nucleation occurs, when

$$G_F = -n_P \tau_o b \tag{6}$$

Take the energy barrier between adjacent equilibrium positions of a dislocation to be G_o^*. An applied shear stress τ has the effect of reducing the height of this barrier [11, 12]:

$$G^* = G_o^* - (\tau - \tau_\mu)v^* \tag{7}$$

where v^* is an activation volume and τ_μ is the temperature independent resistance to dislocation motion. In the context of nucleation, the stress τ is not externally applied but comes from the chemical driving force. On combining the last three equations we obtain [10]:

$$G^* = G_o^* + \left[\tau_\mu + \frac{\rho_A}{b}G_{STRAIN} + \frac{2\sigma}{n_P b}\right]v^* + \frac{\rho_A v^*}{b}\Delta G_{CHEM} \tag{8}$$

It follows that with this model of nucleation the activation energy G^* will decrease *linearly* as the magnitude of the driving force ΔG_{CHEM} increases. This direct proportionality contrasts with the inverse square relationship of classical theory.

The nucleation rate I_V will have a temperature dependence due to the activation energy:

$$I_V \propto \nu \exp\{-G^*/RT\} \tag{9}$$

where ν is an attempt frequency. It follows that

$$-G^* \propto \beta T \qquad \text{where} \qquad \beta = R\ln\{I_V/\nu\} \tag{10}$$

We now assume that there is a specific nucleation rate at T_h, irrespective of the type of steel, in which case β is a constant, negative in value since the attempt frequency should be larger than the actual rate. This gives the interesting result that

$$G_N \propto \beta T \tag{11}$$

which is precisely the relationship observed experimentally, Fig. 12a. This is evidence for nucleation by the dissociation of dislocations with the activation energy proportional to the driving force, as opposed to the inverse square relationship predicted by classical theory. The activation energy G^* in this model comes from the resistance of the lattice to the motion of dislocations.

Nucleation corresponds to a point where the slow, thermally activated migration of glissile partial dislocations gives way to rapid, breakaway dissociation. This is why it is possible to observe two sets of transformation

12

units, the first consisting of very fine embryo platelets below the size of the operational nucleus, and the second the size corresponding to the rapid growth to the final size. Intermediate sizes are rarely observed because the time period for the second stage is expected to be much smaller than that for the first. Figure 13 shows that in addition to the fully grown sub–units (a few micrometers in length), there is another population of much smaller (submicron) particles which represent the embryos at a point in their evolution prior to breakaway.
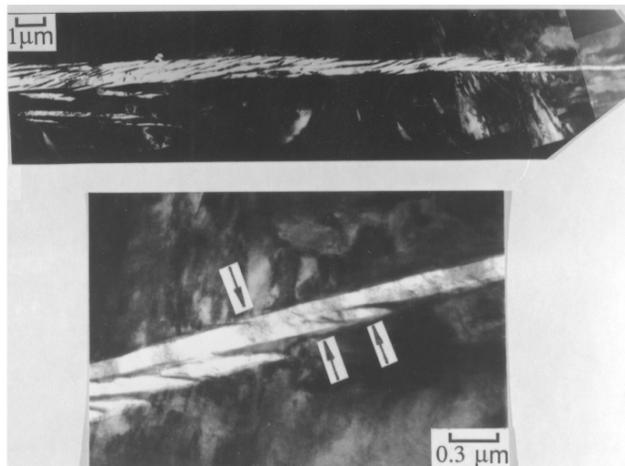
Figure 13: Transmission electron micrograph of a sheaf of bainite in a partially transformed sample. A region near the tip of the sheaf in (a) is enlarged in (b). The arrows in (b) indicate possible sub–operational embryos which are much smaller than the fully grown sub–units seen in (a). After [13]

7   Kinetics of Growth

The rate of the bainite reaction needs to be considered in terms of a number of distinct events (Fig. 14). A sub-unit nucleates at an austenite grain boundary and lengthens at a certain rate before its growth is stifled by plastic deformation within the austenite. New sub-units then nucleate at its tip, and the sheaf structure develops as this process continues. The overall lengthening rate of a sheaf is therefore smaller than that of an individual sub-unit because there is an interval between the formation of successive sub-units. The volume fraction of bainite depends on the totality of sheaves growing from different regions in the sample. Carbide precipitation events also influence the kinetics, primarily by removing carbon either from the residual austenite or from the supersaturated ferrite.

Little is known about the nucleation of bainite except that the activation energy for nucleation is directly proportional to the driving force for transformation. This is consistent with the theory for martensite nucleation. However, unlike martensite, carbon must partition into the austenite during bainite nucleation, although the nucleus then develops into a sub-unit which grows without diffusion.

The scale of individual plates of ferrite is too small to be resolved adequately using optical microscopy, which is capable only of revealing clusters of plates. Using higher-resolution techniques such as photoemission electron microscopy (Fig. 15) it has been possible to study directly the progress of the bainite reaction. Not surprisingly, the lengthening of individual bainite platelets has been found to occur at a rate which is much faster than expected from a diffusion-controlled process. The growth rate is nevertheless much smaller than that of martensite, because the driving force for bainite formation is smaller due to the higher transformation temperatures involved. The platelets tend to grow at a constant rate but are usually stifled before they can traverse the austenite grain.

The lengthening rate of a sheaf is slower still, because of the delay caused by the need to repeatedly nucleate new sub-units. Nevertheless, sheaf lengthening rates are generally found to be about an order of magnitude higher than expected from carbon diffusion-controlled growth. Measurements have also been made of the thickening of bainite sheaves, a process which appears to be discontinuous, the thickness increasing in discrete steps of about $0.5\,\mu$m. These step heights correlate with the size of the sub-units observed using thin-foil
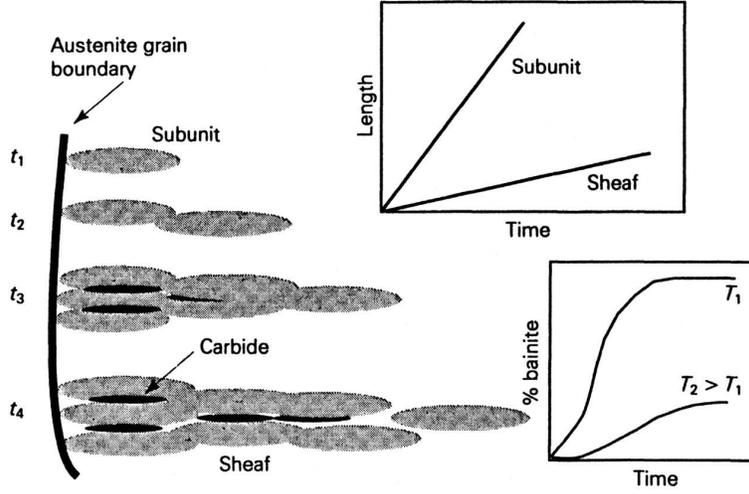
Figure 14: Schematic illustration of the microstructural features relevant in the kinetic description of a bainitic microstructure.

electron microscopy. The thickening process therefore depends on the rate at which sub-units are nucleated in adjacent locations within a sheaf.

The bainitic reaction has several of the recognized features of a nucleation and growth process. It takes place isothermally, starting with an incubation period during which no transformation is detected, followed by an increasing rate of transformation to a maximum and then a gradual slowing down. These features are illustrated in the dilatometric results of Fig. 16, for three transformation temperatures in the bainitic range for a Fe–1Cr–0.4C wt% steel, the extent of transformation increasing with decreasing temperature. In this steel at 510°C the reaction stops after about 1 h, and the remaining austenite is stable at this temperature for a long time.

These overall transformation characteristics, i.e. the change in the fraction of bainite with time, temperature, austenite grain structure and alloy chemistry are therefore best considered in terms of a TTT diagram (Fig. 17). A simplified view is that the TTT diagram consists of two separable C-shaped curves. The one at higher temperatures describes the evolution of diffusional transformation products such as ferrite and pearlite, whereas the lower C-shaped curve represents displacive reactions such as Widmanstätten ferrite and bainite. In lean steels which transform rapidly, these two curves overlap so much that there is apparently just one curve which is the combination of all reactions. As the alloy concentration is increased to retard the decomposition of austenite, the two overlapping curves begin to become distinct, and a characteristic 'gap' develops at about the B_s temperature in the TTT diagram. This gap is important in the design of some high-strength (ausformed) steels which have to be deformed in the austenitic condition at low temperatures before the onset of transformation.

7.1 Simulation of TTT Curves

Assuming the applicability of classical nucleation theory, neglecting strain energy, Russell [15] obtained several expressions for calculating the time τ_s needed to reach a steady–state nucleation rate, for a variety of grain–boundary nucleation phenomena, with the general form:

$$\tau \propto \frac{T}{(\Delta G_m)^p D} \tag{12}$$

where p is an exponent which depends on the nature of the interface between the nucleus and matrix, and D is a diffusion coefficient. If τ_s is empirically identified with the incubation time τ observed for the beginning
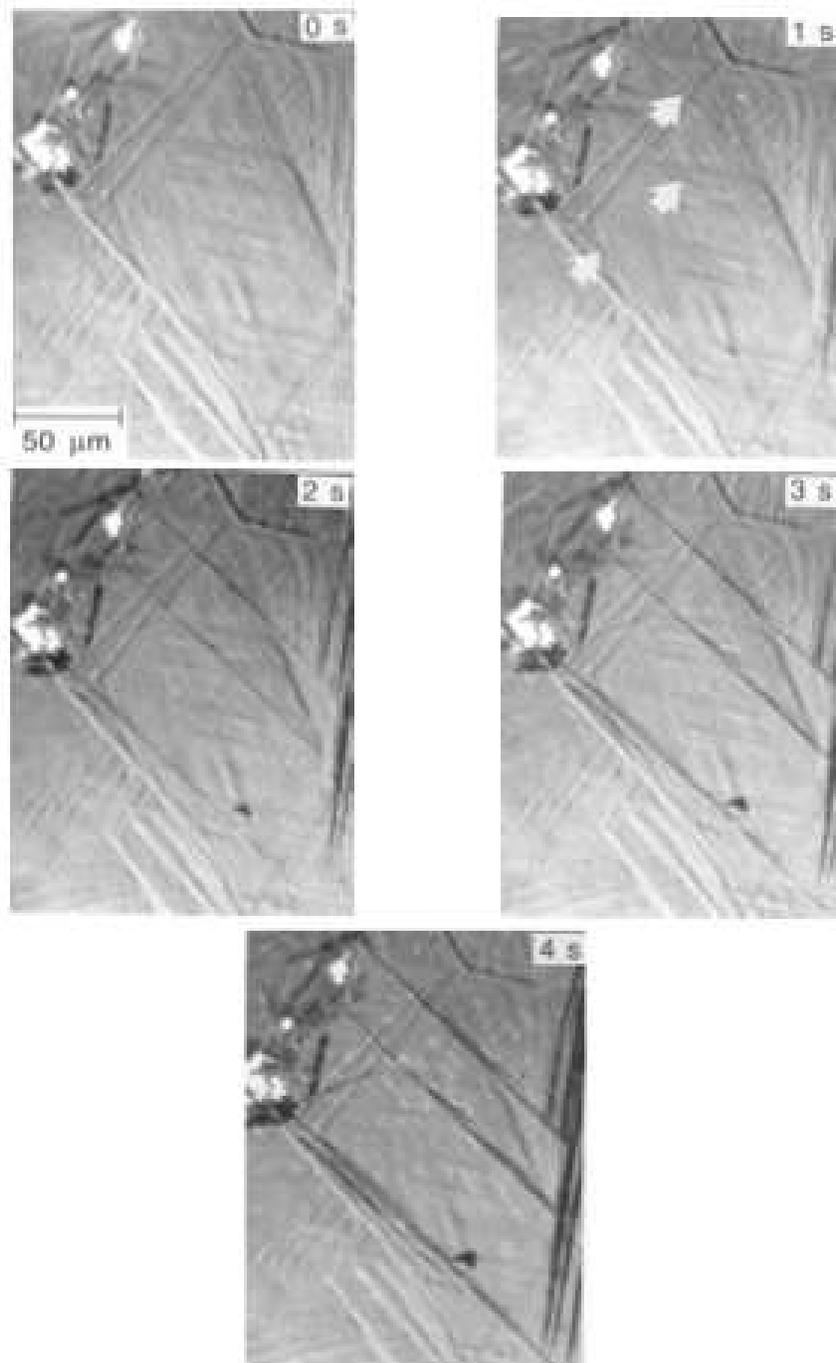
Figure 15: Photoemission electron microscope observations on the growth of individual sub-units in a bainite sheaf. The pictures are taken at 1 s intervals.

of transformation in time–temperature transformation diagrams, then it is possible to establish a reasonable method for calculating the initiation of transformation by generalising equation 12 as follows [16, 17]:

$$\ln\left\{\frac{\tau(\Delta G_m)^p}{T^z}\right\} = \frac{Q'}{RT} + C_4 \tag{13}$$
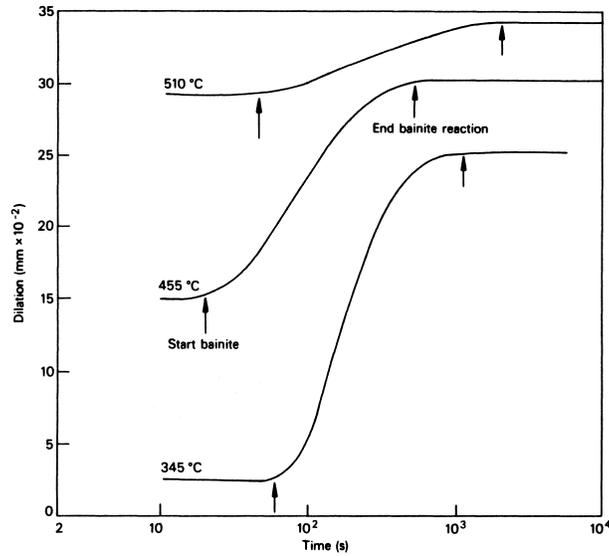
Figure 16: Isothermal reaction curves for the formation of bainite in Fe–1.0Cr–0.4C wt% steel [14].
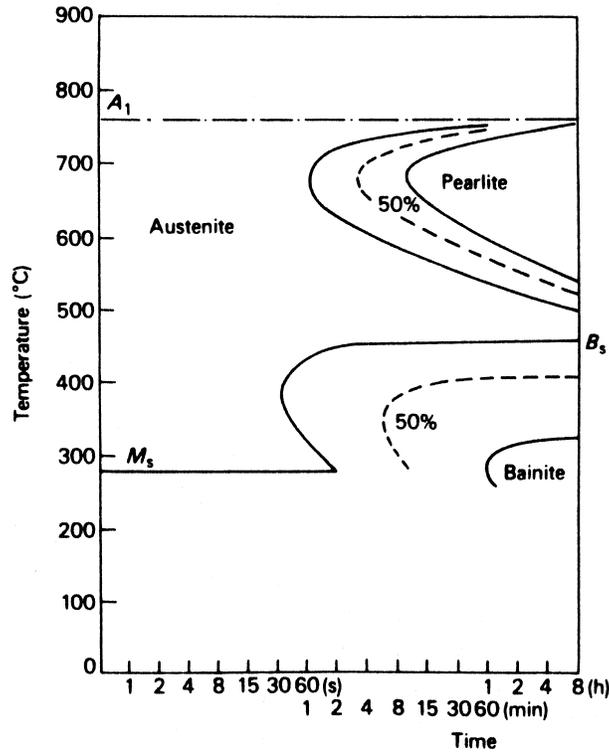
Figure 17: *TTT* curves for a Fe–3Cr–0.5C wt% steel (Thelning, *Steel and its Heat Treatment*, Bofors Handbook, Butterworth, UK, 1975).

where Q', C_4, p and z are obtained by fitting to well–behaved experimental *TTT* diagrams. The method has proved extremely successful in a variety of computer programs, ranging from the design of steel weld metals, steel processing, *etc.* and is available in the public domain under the title MUCG46 [18]. The physical basis

16
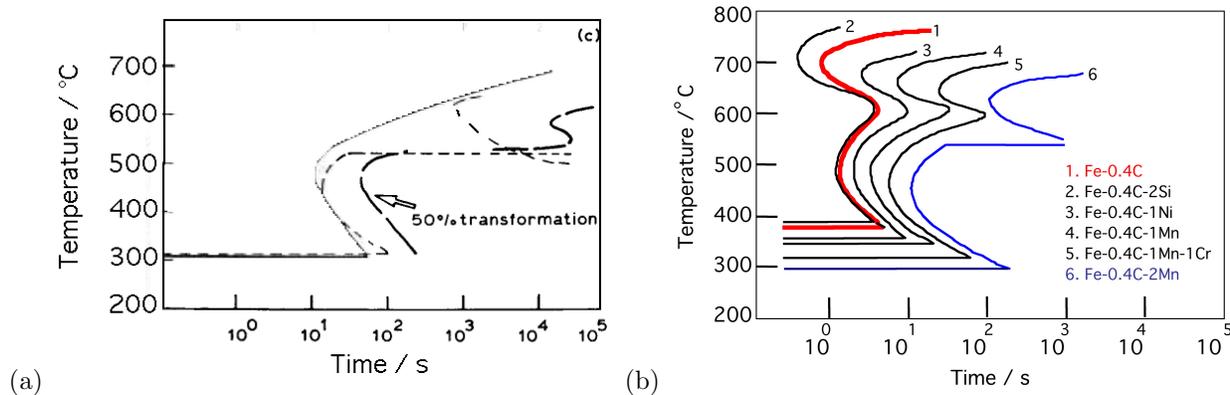
Figure 18: (a) The calculated curve shows a bay, which is incorrectly not present in the corresponding 0% transformation measured–curve, but is evident in the 50% transformation measured–curve, in the correct location. (b) An example set of *TTT* diagram calculations for hypothetical steels. After [16].

of the program is interesting in that it has identified by calculation, a number of errors in published diagrams [16]). An example of such a case is illustrated in Fig. 18a, where the bay is absent in the experimental 0% transformation curve, whereas consistent with the calculation (long dashes), there is a bay in the correct location in the 50% transformation experimental curve.

Since the original work referred to the initiation of the bainite transformation, Takahashi and Bhadeshia [19] extended it to the progress of transformation for steels in which the bainite grows without the precipitation of cementite from austenite. The method nevertheless does not account for the full panoply of theory available. A much more fundamental model has been published recently [20] – however, the comparison with experimental data is limited and intensive research is in progress to properly validate the method and indeed, to integrate the new model into the scheme of solid–state transformations in steels.

Once a *TTT* diagram is obtained, a variety of assumptions can be made to convert it to a continuous cooling transformation diagram. The basis for this is fully described by Christian [21]; for the sake of brevity, the methods are not reviewed here.

8   Transition from Upper to Lower Bainite

As the isothermal transformation temperature is reduced below B_s, lower bainite is obtained in which carbides precipitate in the ferrite, with a correspondingly reduced amount of precipitation from the austenite between the ferrite. This transition from upper to lower bainite can be explained in terms of the rapid tempering processes that occur after the growth of a supersaturated plate of bainite (Fig. 19). Excess carbon tends to partition into the residual austenite by diffusion, but the supersaturation may also be reduced by precipitation in the ferrite.

The time required for a supersaturated plate of ferrite to decarburize by diffusion into austenite is illustrated in Fig. 20 for a typical steel. At elevated temperatures the diffusion is so rapid that there is no opportunity to precipitate carbides in the ferrite, giving rise to an upper bainitic microstructure. Cementite eventually precipitates from the carbon-enriched residual austenite.

As the transformation temperature is reduced and the time for decarburization increases, some of the carbon has an opportunity to precipitate as fine carbides in the ferrite, whereas the remainder partitions into the austenite, eventually to precipitate as inter-plate carbides. This is the lower bainite microstructure. Because only a fraction of the carbon partitions into the austenite the inter-plate carbides are much smaller than those associated with upper bainite. This is why lower bainite with its highly refined microstructure is always

17
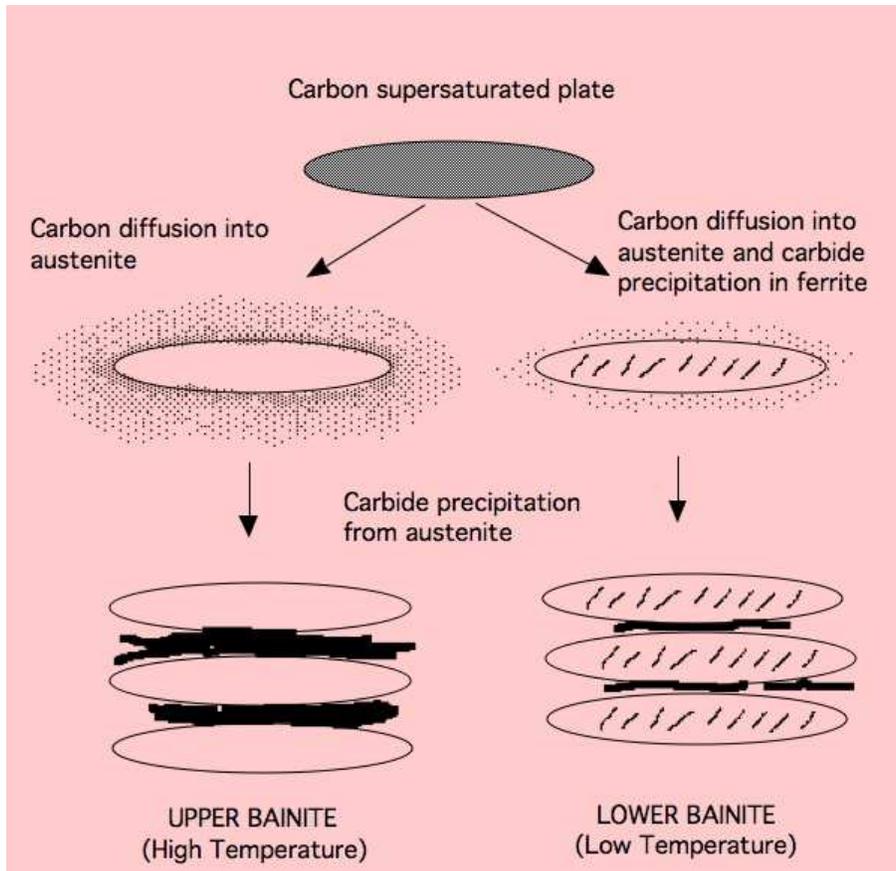
Figure 19: Schematic representation of the transition from upper to lower bainite.

found to be much tougher than upper bainite, even though it usually has a much higher strength.

A corollary to the mechanism of the transition from upper to lower bainite is that in steels containing high concentrations of carbon, only lower bainite is ever obtained. The large amount of carbon that is trapped in the ferrite by transformation simply cannot escape fast enough into the austenite so that precipitation from ferrite is unavoidable. Conversely, in very low-carbon steels, the time for decarburization is so small that only upper bainite is obtained by transformation at all temperatures between the pearlite-finish and the martensite-start temperatures.

It is also possible to obtain mixtures of upper and lower bainite by isothermal transformation. As upper bainite forms first, the residual austenite becomes richer in carbon and the tendency to form lower bainite increases as the transformation progresses.

9   Granular Bainite

Granular bainite (Fig. 21) is a term frequently used to describe the bainite that occurs during continuous cooling transformation. This terminology is used widely in industry, where most steels undergo non-isothermal heat treatments. A good example is the energy generation industry where larger Cr–Mo steel components are allowed to cool naturally from the austenitic state, to generate bainitic microstructures.

Granular bainite cannot readily be distinguished from ordinary bainite when examined using transmission electron microscopy, because its mechanism of formation is not different. However, because the microstruc-
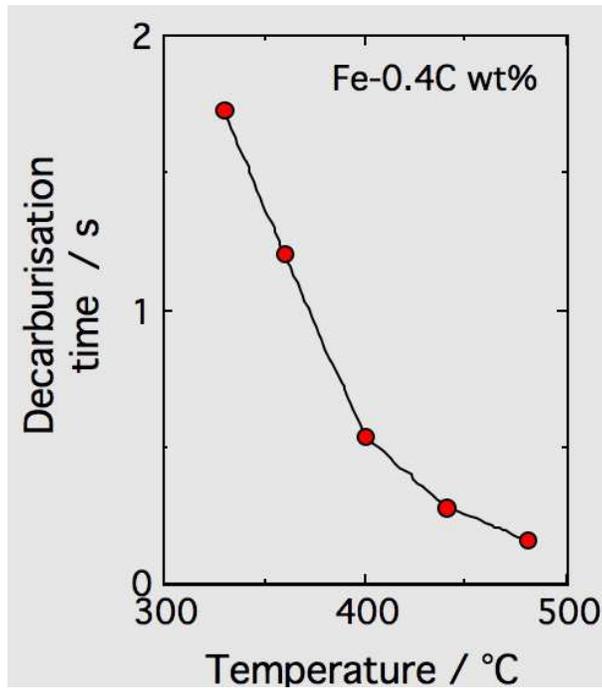
Figure 20: The approximate time required to decarburize a supersaturated plate of bainite.
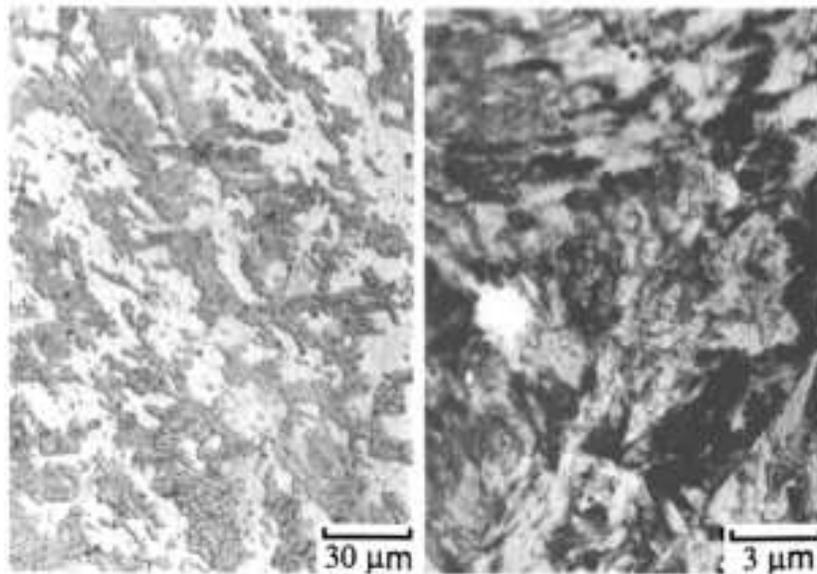
Figure 21: Granular bainite in a Fe–0.15C–2.25Cr–0.5Mo wt% steel of the kind used extensively in the energy generation industry. (a) Light micrograph. (b) Corresponding transmission electron micrograph (after Joseffson, 1989).

ture forms gradually during cooling, the sheaves of bainite can be rather coarse. The optical microstructure then gives the appearance of blocks of bainite and austenite, so that it is appropriate to use the adjective 'granular'.

A characteristic (though not unique) feature of granular bainite is the lack of carbides in the microstructure. Instead, the carbon that is partitioned from the bainitic ferrite stabilizes the residual austenite, so that the final microstructure contains both retained austenite and some high-carbon martensite in addition to the bainitic ferrite.

10   Tempering of Bainite

The extent and the rate of change of the microstructure and properties during tempering must depend on how far the initial sample deviates from equilibrium. The behaviour of bainite during tempering is therefore expected to be different from that of martensite.

Unlike martensite, bainitic ferrite usually contains only a slight excess of carbon in solution. Most of the carbon in a transformed sample of bainite is in the form of cementite particles, which in turn tend to be coarser than those associated with tempered martensite. The effects of tempering heat treatments are therefore always milder than is the case when martensite in the same steel is annealed.

Bainite forms at relatively high temperatures where some recovery occurs during transformation. Consequently, when low-carbon bainitic steels are annealed at temperatures as high as 700°C (1 h), there are only minor changes in recovery, morphology or carbide particles. Rapid softening occurs only when the plate-like structure of ferrite changes into equi-axed ferrite. Associated with this change is the spherodization and coarsening of cementite. Further tempering has minimal effects.

In marked contrast with martensitic steels, small variations in the carbon concentration (0.06–0.14 wt%) have little effect on the tempering of bainite. Carbon has a very potent solid solution strengthening effect. Thus, the strength of martensite drops sharply as the carbon precipitates during tempering. With bainite the carbon is mostly present as coarse carbides which contribute little to strength. It is not therefore surprising that the tempering response is rather insensitive to the bulk carbon concentration.

Many bainitic microstructures contain appreciable quantities of retained austenite. Tempering, usually at temperatures in excess of 400°C, induces the decomposition of this austenite into a mixture of ferrite and carbides.

Bainitic steels containing strong carbide-forming elements such as Cr, V, Mo and Nb, undergo secondary hardening during annealing at high temperatures. Secondary hardening occurs when fine (more stable) alloy carbides form at the expense of cementite. Because the cementite in bainite is coarse, the secondary hardening reaction tends to be sluggish when compared with martensite.

There is considerable interest in the use of copper-bearing bainitic steels for applications in heavy engineering. Tempering induces the formation of fine particles of copper which contribute to strength without jeopardizing toughness.

To summarize, there are significant differences in the tempering behaviour of bainite and martensite, the most prominent being that there is little carbon in solid solution in bainite. This has the consequence that bainitic microstructures are much less sensitive to tempering, since there is hardly any loss of strength due to the removal of the small quantity of dissolved carbon. Major changes in strength occur only when the bainite plate microstructure coarsens or recrystallizes into one consisting of equi-axed grains of ferrite. Minor changes in strength are due to cementite particle coarsening and a general recovery of the dislocation substructure. Bainitic steels containing strong carbide-forming elements tend to exhibit secondary hardening phenomena rather like those observed in martensitic steels which depends on the precipitation of fine alloy carbides.

11   Alloying Elements

Carbon has a large effect on the range of temperature over which upper and lower bainite occur. The B_s temperature is depressed by many alloying elements but carbon has the greatest influence, as indicated by the following empirical equation:

$$B_s(^\circ\mathrm{C}) = 830 - 270\mathrm{C} - 90\mathrm{Mn} - 37\mathrm{Ni} - 70\mathrm{Cr} - 83\mathrm{Mo},$$

where the concentrations are all in wt%. Carbon has a much larger solubility in austenite than in ferrite, and is a very powerful austenite stabilizer which leads to a general retardation of reaction kinetics. The fraction of carbides to be found in the final microstructure increases in proportion to the carbon concentration, so that the concentration must be kept below about 0.4 wt% to ensure reliable mechanical properties. We have already seen that an increase in carbon makes it easier for lower bainite to form because it becomes more difficult for plates of supersaturated bainitic ferrite to decarburize before the onset of cementite precipitation. In plain carbon steels, the bainitic reaction is kinetically shielded by the ferrite and pearlite reactions which commence at higher temperatures and shorter times (Fig. 18b), so that in continuously cooled samples bainitic structures are difficult to obtain. Even using isothermal transformation, difficulties arise if, e.g., the ferrite reaction is particularly rapid. The addition of metallic alloying elements usually results in the retardation of the ferrite and pearlite reactions. In addition, the bainite reaction is depressed to lower temperatures. This often leads to a greater separation of the reactions, and the TTT curves for many alloy steels show much more clearly separate C-shaped curves for the pearlite and bainitic reactions (Fig. 18b). However, it is still difficult to obtain a fully bainitic microstructure because of its proximity to the martensite reaction.

A very effective means of isolating the bainite reaction in low-carbon steels has been found by adding about 0.002 wt% soluble boron to a Ohm wt% Mo steel. While the straight molybdenum steel encourages the bainite reaction, the boron markedly retards the ferrite reaction, probably by preferential segregation to the prior austenite boundaries. This permits the bainite reaction to occur at shorter times. At the same time, the bainite C-shaped curve is hardly affected by the boron addition, so that martensite formation is not enhanced. Consequently, by the use of a range of cooling rates, fully bainitic steels can be obtained.

12   Use of Bainitic Steels

There are large markets for steels with strengths less than 1000 MPa, and where the total alloy concentration rarely exceeds 2 wt%. Bainitic steels are well suited for applications within these constraints. However, alloy design must be careful in order to obtain the right microstructures. Steels with inadequate hardenability tend to transform to mixtures of allotriomorphic ferrite and bainite. Attempts to improve hardenability usually lead to partially martensitic microstructures. The solution therefore lies in low-alloy, low-carbon steels, containing small amounts of boron and molybdenum to suppress allotriomorphic ferrite formation. Boron increases the bainitic hardenability. Other solute additions can, in the presence of boron, be kept at sufficiently low concentrations to avoid the formation of martensite. A typical composition might be Fe–0.1C–0.25Si–0.50Mn–0.55Mo–0.003B wt%. Steels like these are found to transform into virtually fully bainitic microstructures with very little martensite using normalizing heat treatments.

The most modern bainitic steels are designed with much reduced carbon and other alloying element concentrations. They are then processed using accelerated cooling in order to obtain the necessary bainitic microstructure. The reduced alloy concentration not only gives better weldability, but also a larger strength due to the refined bainitic microstructure.

The range of bainitic alloys available commercially is summarized in Fig. 22, and some typical alloy compositions are stated in Table 1. The ultra-high-strength steels consist of mixtures of bainite ferrite, martensite and retained austenite. They have an enhanced hardenability using manganese, chromium and nickel, and usually also contain a large silicon concentration ($\sim$2 wt%) in order to prevent the formation of cementite.
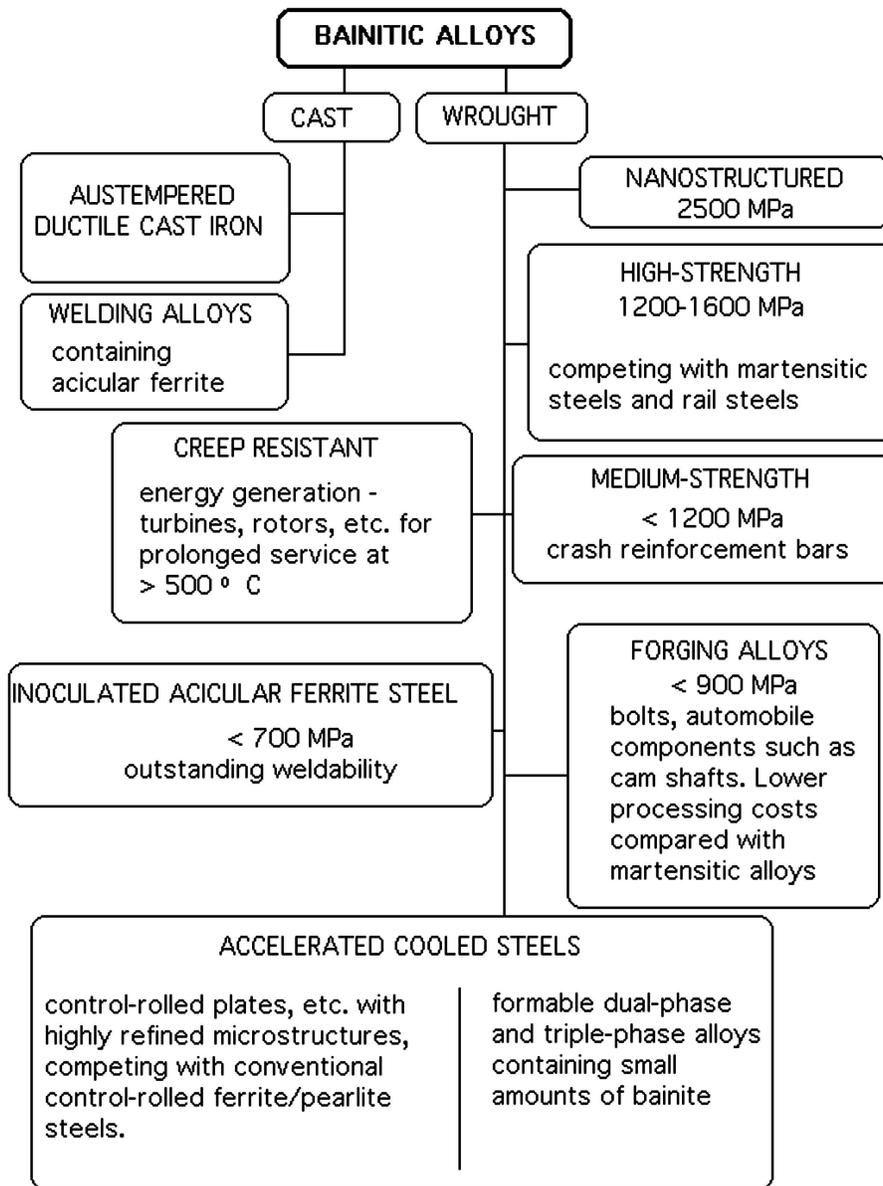
Figure 22: Bainitic alloys currently available commercially.

High-strength steels are made with very low impurity and inclusion concentrations, so that the steel then becomes susceptible to the formation of cementite particles, which therefore have to be avoided or refined.

Medium-strength steels with the same microstructure but somewhat reduced alloy content have found applications in the automobile industry as crash reinforcement bars to protect against sidewise impact. Another major advance in the automobile industry has been in the application of bainitic forging alloys to the manufacture of components such as cam shafts. These were previously made of martensitic steels by forging, hardening, tempering, straightening and finally stress-relieving. All of these operations are now replaced by controlled cooling from the die forging temperature, to generate the bainitic microstructure, with cost savings which on occasions have made the difference between profit and loss for the entire unit.

Creep-resistant bainitic steels have been used successfully in the power generation industry since the early

1940s. Their hardenability has to be such that components as large as 1 m in diameter can be cooled continuously to generate a bainitic microstructure throughout the section. The alloys utilize chromium and molybdenum, which serve to enhance hardenability but also, during subsequent heat-treatment, cause the precipitation of alloy carbides which greatly improve the creep resistance.

Table 1: Chemical composition, wt%, of typical bainitic steels

Alloy	C	Si	Mn	Ni	Mo	Cr	V	B	Nb	Other
Early bainite	0.10	0.25	0.5	–	–	0.003	–	–	–	
Low carbon	0.02	0.20	2.0	0.3	0.30	–	–	0.010	0.05	
Strong	0.20	2.00	3.0	–	–	–	–	–	–	
Creep resistant	0.15	0.25	0.50	–	1.00	2.30	–	–	–	
Forging alloy	0.10	0.25	1.00	0.50	1.00	–	–	–	0.10	
Inoculated	0.08	0.20	1.40	–	–	–	–	–	0.10	0.012 Ti
Nanostructured	1.0	1.50	1.90	–	0.26	1.26	0.1	–	–	

By inoculating molten steel with controlled additions of non-metallic particles, bainite can be induced to nucleate intragranularly on the inclusions, rather than from the austenite grain surfaces. This intragranularly nucleated bainite is called 'acicular ferrite'. It is a much more disorganized microstructure with a larger ability to deflect cracks. Inoculated steels are now available commercially and are being used in demanding structural applications such as the fabrication of oil rigs for hostile environments.

Advances in rolling technology have led to the ability to cool the steel plate rapidly during the rolling process, without causing undue distortion. This has led to the development of 'accelerated cooled steels' which have a bainitic microstructure, can be highly formable and compete with conventional control-rolled steels.

13   Nanostructured Bainite

It would be nice to have a strong material which can be used for making components which are large in all their dimensions, and which does not require mechanical processing or rapid cooling to reach the desired properties. The following conditions are required to achieve this:

(i) The material must not rely on perfection to achieve its properties. Strength can be generated by incorporating a large number density of defects such as grain boundaries and dislocations, but the defects must not be introduced by deformation if the shape of the material is not to be limited.

(ii) Defects can be introduced by phase transformation, but to disperse them on a sufficiently fine scale requires the phase change to occur at large undercoolings (large free energy changes). Transformation at low temperatures also has the advantage that the microstructure becomes refined.

(iii) A strong material must be able to fail in a safe manner. It should be tough.

(iv) Recalescence limits the undercooling that can be achieved. Therefore, the product phase must be such that it has a small latent heat of formation and grows at a rate which allows the ready dissipation of heat.

Recent discoveries have shown that carbide-free bainite can satisfy these criteria [22]. Bainite and martensite are generated from austenite without diffusion by a displacive mechanism. Not only does this lead to solute-trapping but also a huge strain energy term, both of which reduce the heat of transformation. The growth of individual plates in both of these transformations is fast, but unlike martensite, the *overall rate* of reaction is much smaller for bainite. This is because the transformation propagates by a sub-unit mechanism in which the rate is controlled by nucleation rather than growth. This mitigates recalescence.

The theory of the bainite transformation allows the estimation of the lowest temperature at which bainite can be induced to grow [4]. Such calculations are illustrated in Fig. 23a, which shows how the bainite-start (B_s) and martensite-start (M_s) temperatures vary as a function of the carbon concentration, in a particular alloy system. There is in principle no lower limit to the temperature at which bainite can be generated. On the other hand, the rate at which bainite forms slow down dramatically as the transformation temperature is reduced (Fig. 23b). It may take hundreds or thousands of years to generate bainite at room temperature. For practical purposes, the carbon concentration has to be limited to about 1 wt% for the case illustrated.
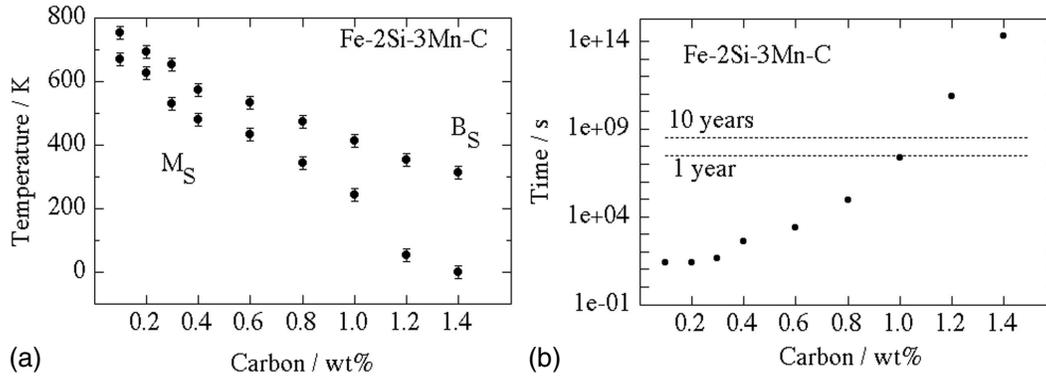
Figure 23: (a) Calculated transformation start temperatures in Fe–2Si–3Mn wt% steel as a function of the carbon concentration. (b) The calculated time required to initiate bainite at the B_S temperature.

An alloy has been designed in this way, with the approximate composition Fe–1C–1.5Si–1.9Mn–0.25Mo–1.3Cr–0.1V wt%, which on transformation at 200°C, leads to bainite plates which are only 20–40 nm thick. The slender plates of bainite are dispersed in stable carbon-enriched austenite which, with its face-centred cubic lattice, buffers the propagation of cracks (Fig. 24).
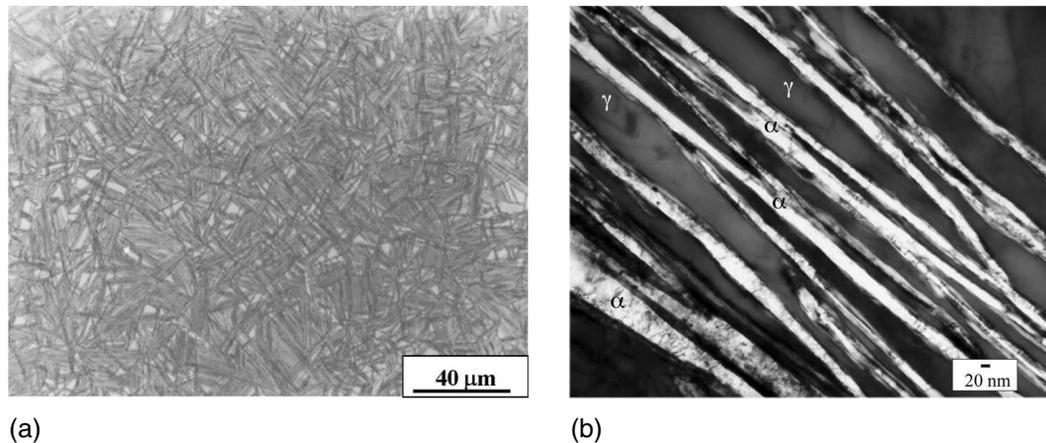
Figure 24: (a) Optical micrograph. (b) Transmission electron micrograph (Caballero, Mateo and Bhadeshia).

The bainite obtained by transformation at very low temperatures is the hardest ever (700 HV, 2500 MPa), has considerable ductility, is tough (30–40 MPa m$^{1/2}$) and does not require mechanical processing or rapid cooling.

The steel after heat treatment therefore does not have long-range residual stresses, it is very cheap to produce and has uniform properties in very large sections. In effect, the hard bainite has achieved all of the essential objectives of structural nanomaterials which are the subject of so much research, but in large dimensions.

14 Mechanical Properties

14.1 Strength

It is reasonable to assume that the strength of martensite and bainite can be factorized into a number of intrinsic components:

$$\sigma = \sigma_{Fe} + \sum_i x_i \sigma_{SS_i} + \sigma_C + K_L(\overline{L})^{-1} + K_D \rho_D^{0.5}, \tag{14}$$

where x_i is the concentration of a substitutional solute which is represented here by a subscript i. The other terms in this equation can be listed as follows:

$K_L =$ coefficient for strengthening due to lath size, $115 \, \mathrm{MN \, m^{-1}}$
$K_D =$ coefficient for strengthening due to dislocations, $7.34 \times 10^{-6} \, \mathrm{MN \, m^{-1}}$
$\sigma_{Fe} =$ strength of pure, annealed iron, $219 \, \mathrm{MN \, m^{-2}}$ at $300 \, \mathrm{K}$
$\sigma_{SSi} =$ substitutional solute (i) strengthening
$\sigma_c =$ solid solution strengthening due to carbon
$\rho_D =$ dislocation density, typically $10^{16} \, \mathrm{m^{-2}}$
$\overline{L} =$ measure of the ferrite plate size, typically $0.2 \, \mu\mathrm{m}$.

The individual strengthening contributions are discussed below.

Table 2: Strength ($\mathrm{MN \, m^{-2}}$) of pure iron as a function of temperature and solid solution strengthening terms for ferrite, for one wt% of solute. The data are for a strain rate of $0.0025 \, \mathrm{s^{-1}}$

	200°C	100°C	Room temperature (23°C)	−40°C	−60°C
Fe	215	215	219	355	534
Si	78	95	105	70	−44
Mn	37	41	45	8	−57
Ni	19	23	37	−2	−41
Mo	–	–	18	–	–
Cr	7.8	5.9	5.8	7.4	15.5
V	–	–	4.5	–	–
Co	1.0	1.8	4.9	9.1	5.8

14.1.1 Iron and substitutional solutes

Pure body-centred cubic iron in a fully annealed condition makes an intrinsic contribution σ_{Fe} to the overall strength. Substitutional solutes do not partition during the displacive growth of either martensite or bainite, so that their concentrations are fixed by the composition of steel as a whole. Solid solution strengthening contributions, σ_{SSi} can be estimated as a function of temperature and strain rate from published data. Table 2 shows that whereas the strength of pure iron increases as the temperature is reduced, strengthening due to substitutional solutes often goes through a maximum as a function of temperature. Indeed, there is some solution softening at low temperatures because the presence of a foreign atom locally assists a dislocation to overcome the Peierls barrier at low temperatures.

14.1.2 Carbon

Bainitic ferrite has only a small amount of carbon dissolved in interstitial solution, assumed to be less than 0.02 wt%. Martensite, on the other hand, can have concentrations well in excess of $\overline{x}$ (the average

concentration of the alloy), since the prior formation of bainite enriches the residual austenite according to the following relationship derived from a balance of mass. The total carbon concentration in the alloy ($\overline{x}$) is the sum of the concentrations in the austenite (x_γ) and bainitic ferrite (x_b):

$$\overline{x} = x_\gamma V_\gamma + x_b V_b, \tag{15}$$

where V_γ and V_b are the volume fractions of austenite and bainitic ferrite, respectively. It follows that:

$$x_\gamma = \frac{\overline{x} - V_b x_b}{1 - V_b}, \tag{16}$$

x_γ is the concentration in the residual austenite before it transforms into martensite, so that its value is important in determining the hardness of the martensite. Solid-solution theory indicates that the strength increment due to dissolved carbon should vary with the square root of the carbon concentration:

$$\sigma_{SS_C} = 1722.5 \times x^{1/2}, \tag{17}$$

where strength is in $\mathrm{MN\,m^{-2}}$ and the concentration x is expressed in wt%.

14.1.3 Dislocations

When martensite or bainite form at high temperatures, the shape change due to shear transformation causes plastic deformation, and hence the accumulation of dislocations in both the parent and product phases. The extent of the plasticity depends on the yield strength, and hence on the temperature. Takahashi and Bhadeshia [23] have therefore suggested that the dislocation density (ρ_D) of both martensite and bainite can be represented empirically as a function of temperature alone, for the temperature range 570–920 K:

$$\log_{10}\{\rho_D\} = 9.2840 + \frac{6880.73}{T} - \frac{1780360}{T^2}, \tag{18}$$

where T is the transformation temperature in Kelvin, and ρ_D is stated in units of $\mathrm{m^{-2}}$. The strengthening σ_ρ ($\mathrm{MN\,m^{-2}}$) due to dislocations is given by:

$$\sigma_\rho = 0.38\,\mu b (\rho_D)^{0.5} \simeq 7.34 \times 10^{-6} (\rho_D)^{0.5}, \tag{19}$$

where μ is the shear modulus and b is the magnitude of the Burgers vector.

14.1.4 Lath size

Martensite and bainite grow in the form of very fine plates or laths. The resulting grain size strengthening σ_G is defined as:

$$\sigma_G \simeq 115(\overline{L})^{-1}\,\mathrm{MN\,m^{-2}}, \tag{20}$$

where $\overline{L}$ (μm) is the mean linear intercept measured on random sections. This is not the classical Hall–Petch relation but another relation due to Langford and Cohen, because at the typically sub-micrometre grain sizes, the mechanism of yield is different, involving the initiation of dislocation sources in the grain boundaries.

14.1.5 Martensite composition and transformation temperature

The excess carbon in the bainitic ferrite partitions into the residual austenite, which then transforms to martensite. The carbon concentration of the martensite can therefore be calculated from a simple mass balance (Equation (14.11)). The martensite-start temperature (M_S) of the residual austenite can be written:

$$M_S = M_S^0 - 564(x_\gamma - \overline{x}), \tag{21}$$

26

where the concentrations are in wt%, the temperatures in centigrade and M_S^0 is the martensite-start temperature of austenite with the average composition of the alloy.

The different contributions to the strength of martensite are illustrated in Fig. 25. Carbon is a major contributor since it causes a severe, asymmetrical distortion of the martensite crystal structure and hence interacts strongly with the movement of dislocations. The dislocation density itself makes a significant contribution to the overall strength.
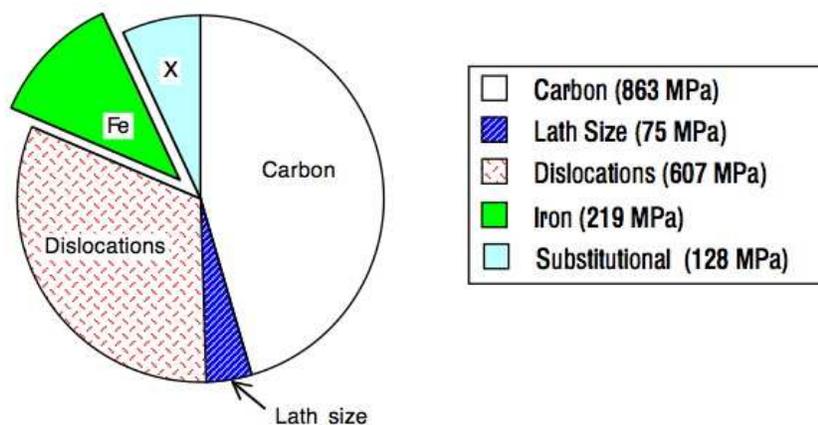
Figure 25: Calculated components of the room-temperature strength of virgin martensite in Fe–0.4C–0.2Si–0.71Mn–1.9Ni–0.25Mo–0.88Crwt% alloy. This is a typical ultra-high-strength steel of the type used in the manufacture of gears, gun barrels, etc.

14.1.6 Strength of mixed microstructures

The normal way to calculate the strength of a multiphase alloy is to use a rule of mixtures, i.e. to calculate a mean strength from the strength of each component phase weighted by its volume fraction. However, this is not adequate for the present purposes because of constraint effects. It is well established in fracture mechanics that the yield strength is increased by plastic constraint. This is why a weak brazing alloy can be used to effectively bond much stronger samples, as long as the thickness of the braze material is small enough to be constrained throughout by the surrounding stronger matrix. Indeed, the strength of the joint increases as the thickness of the braze layer decreases.

Dispersions of bainite plates form in austenite which subsequently transforms to much stronger martensite. Young, therefore, assumed that deformation of the bainitic ferrite is constrained by the harder martensite in the same way as the braze material is constrained by the surrounding matrix. The constraint can, therefore, be modelled using experimental data available from brazed joints in high-strength steels. The brazing alloys used in making the joints were non-ferrous materials which are ordinarily rather weak. The data, in a normalized form, are summarized in Fig. 26. The vertical axis is the joint strength normalized with respect to that of the unconstrained braze material; the horizontal axis is the braze thickness normalized relative to a thickness value where the restraint effect vanishes.

To analyse the properties of a mixed microstructure, it can be assumed that the normalized braze thickness is equivalent to the volume fraction of bainite. Using this assumption, and the form of the normalized strength versus normalized thickness plot (Fig. 26), the strength of constrained bainite may be represented by the equation:

$$\sigma \simeq \sigma_0[0.65\exp\{-3.3V_b\} + 0.98] \leq \sigma_M, \tag{22}$$

where σ and σ_0 represent the strengths of constrained and unconstrained bainite, respectively, σ_M is the
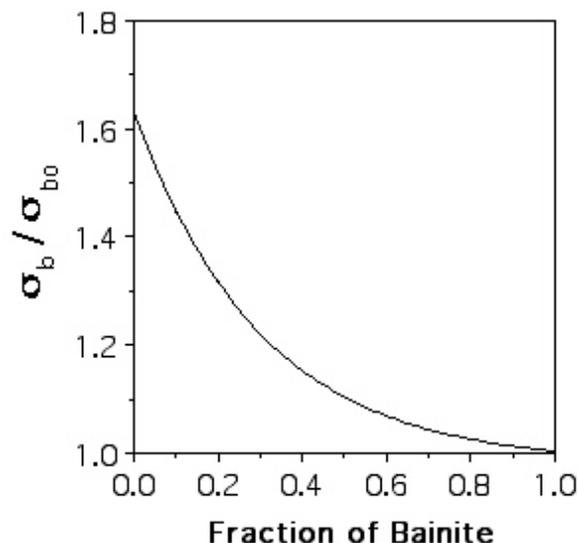
Figure 26: Plot of the normalized strength of a brazed joint versus the normalized thickness of the brazing material, the latter being identified with the fraction of bainite in a martensitic matrix [24].

strength of the martensite and V_b is the volume fraction of the bainite. The strength of bainite is always less than or equal to that of martensite.

When the volume fraction V_b of bainite is small, its strength nearly matches that of martensite (Fig. 27a), always remaining above that of bainite on its own. The strength of martensite continues to increase with the fraction of bainite, as the carbon concentration of the residual austenite from which it grows, increases.

Figure 27b shows how the strength of the mixed microstructure is predicted. Line (a) on Fig. 27b shows that a rule of mixtures cannot account properly for the variations observed. The agreement between calculation and experiment improves (curve b) as allowance is made for the change in the strength of martensite as carbon partitions into the austenite, due to the formation of bainite. The consistency between experiment and theory becomes excellent as constraint effects are also included in the calculations (curve c).

14.2   Ductility

A high density of internal surfaces is not always good for a steel. This is because the boundaries either act as sinks for dislocations or there is insufficient room for dislocation multiplication mechanisms to operate. As a consequence there is no mechanism for work hardening and nanostructured materials therefore suffer from plastic instability soon after yielding [26, 27]. Indeed, in one experiment, a nanostructured ferrite when forced to shear failed to deform by ordinary mechanisms and instead underwent displacive transformation to austenite at room temperature as a way of accommodating the applied stress [28].

The motivation for ever finer grain sizes comes from a desire for stronger materials. Work–hardening must therefore be introduced into nanostructured materials to avoid plastic instabilities and hence enable the exploitation of strength. This has been achieved in a wonderful steel by introducing retained austenite between plates of bainite, each of which is thinner than a typical carbon nanotube [29, 22, 30, 31, 32, 33, 34], Fig. 28. Notice that although the thickness of the plates is of the order of 20–40 nm, their length is much longer. Nevertheless, the mean slip distance through a plate is about twice the thickness, so in spite of the anisotropy of shape, this can, from a strength point of view, be classified as a nanostructured metal. The mixture of large and small dimensions is an advantage over equiaxed grains in giving a much greater amount of surface per unit volume within the bulk [35].

28
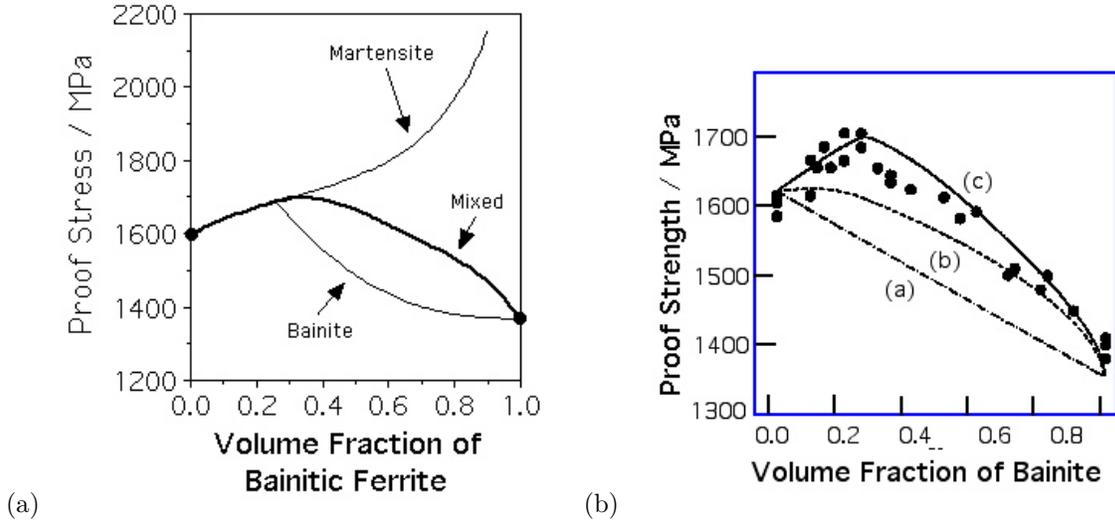
Figure 27: (a) The strength contributions of bainite and martensite in the mixed microstructure. (b) Comparison of calculations against experimental data due to [25].

In this microstructure, the austenite transforms into martensite under the influence of applied stress and this results in work hardening, with large and almost completely uniform plastic strain Fig. 29, details listed in Table 3. What then determines the fracture strain?
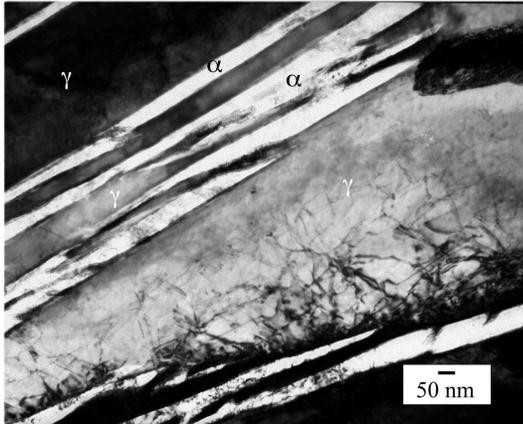
Figure 28: Fe-0.98C-1.46Si-1.89Mn-0.26Mo-1.26Cr-0.09V wt%, transformed at 200°C for 5 days. Transmission electron micrograph [22, 29, 31].

The change in the austenite content with plastic strain and the driving force for martensitic transformation can be estimated as shown in Fig. 30 for the cases listed in Table 3 [37]. Also plotted are points which define in each case the strain at which the tensile samples failed. A prominent feature is that they all fail when the retained austenite content is reduced to about 10%. An experimental study by Sherif [38] on an aluminium–free alloy which is otherwise identical to the steel considered here, is consistent with this conclusion. His X–ray studies also indicated that tensile failure in nanostructured bainite occurs when the retained austenite content is diminished to about 10%.

This observation can be understood if it is assumed that failure occurs when the austenite, which is the toughest of all the phases present, becomes geometrically isolated, *i.e.,* it loses percolation, leading to fracture. Garboczi *et al.* have developed a numerical model for the percolation threshold when freely overlapping objects (general ellipsoids) are placed in a matrix [39]. Since the austenite is subdivided roughly into the form of plates by the bainite, it can be represented by oblate ellipsoids with an aspect ratio r of between

29

T_I / °C	V_γ	σ_Y / GPa	σ_{UTS} / GPa	Elongation / %
200	0.17	1.41	2.26	7.6
300	0.21	1.40	1.93	9.4
400	0.37	1.25	1.7	27.5

Table 3: T_I, V_γ, σ_Y and σ_{UTS} stand for isothermal transformation temperature, the volume fraction of retained austenite, the 0.2% proof and ultimate tensile strengths respectively [36].
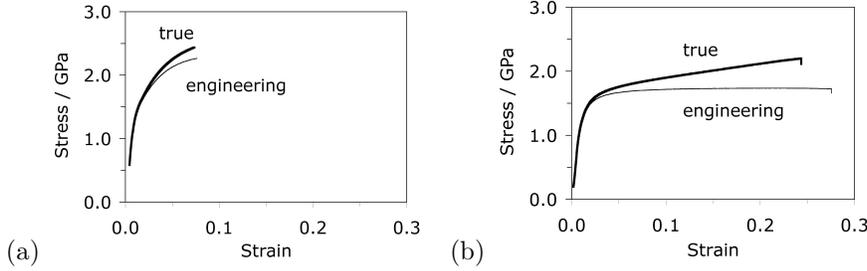
Figure 29: Fe–0.79C–1.56Si–1.98Mn–0.24Mo–1.01Cr–1.51Co–1.01Al wt%. True and engineering stress–strain curves. (a) Bainite generated by transformation at 200°C. (b) Bainite generated by transformation at 300°C. Data from [36].
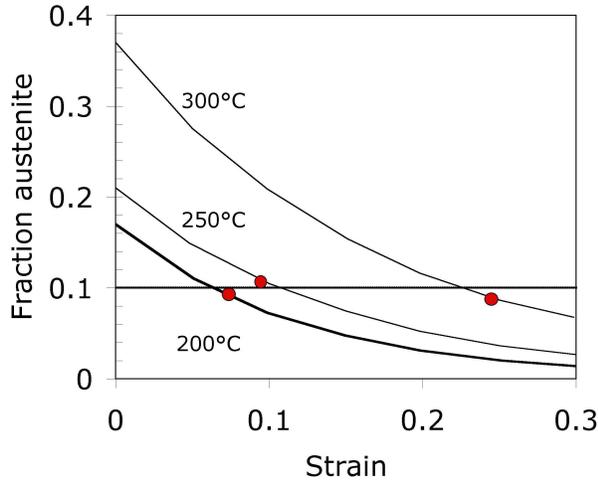
Figure 30: Calculated variation in the fraction of austenite as a function of plastic strain for the samples listed in Table 2. Also marked are points indicating the measured fracture strain for each case. Fracture seems to occur when the austenite content decreases to about 10% of the microstructure. Data adapted from [36].

about 1/10 and 1/100. The percolation threshold is then found to be $p_c \simeq 1.27r$, *i.e.*, $0.127 \geq p_c \geq 0.0127$. This is consistent with the observation that tensile failure occurs when $V_\gamma \simeq 0.1$.

It seems then that the formation of hard, stress/strain–induced martensite can only be tolerated if the austenite maintains a continuous path through the test sample.

14.3 Toughness

Because of the difference in the mechanism of transformation, bainitic steels have always been second–best when compared with tempered martensite. The lack of toughness can in principle be eliminated by using steels with a high silicon concentration (e.g., 1.5 wt%). Silicon has a negligible solubility in cementite and hence greatly retards its precipitation.
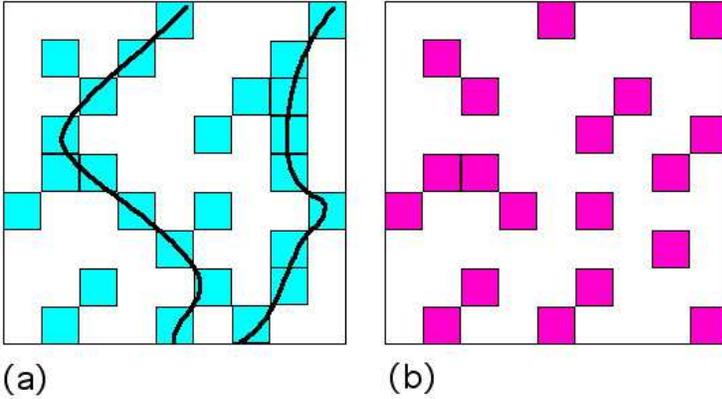
Figure 31: An illustration of percolation. In (a) the coloured phase has a fraction beyond the percolation threshold and in (b) it is below that threshold.

The transformation stops before the final stage illustrated in Fig. 32 is reached, leaving at the isothermal transformation temperature, plates of bainitic ferrite separated by films of carbon–enriched austenite (Fig. 32a). There are no cementite particles to nucleate cleavage cracks or voids; the bainitic ferrite has a low concentration of dissolved carbon; strengthening and toughening is achieved by the very fine ferrite plates (a natural consequence of the transformation mechanism); there are intimately–mixed ductile films of austenite to blunt any cracks and perhaps to toughen via a TRIP effect; the austenite also impedes penetration of the steel by hydrogen. Evidently, a dream microstructure.

Unfortunately, this seemingly ideal microstructure does not live up to expectations. There are, in addition to the films of austenite, some large "blocky" regions of austenite in the microstructure (Fig. 32). The blocks are relatively unstable and transform into high–carbon, untempered, brittle–martensite under the influence of stress. These large "inclusions" render the steel brittle. They are a direct consequence of the mechanism of transformation. We have noted earlier that bainite grows without diffusion (although the excess carbon is then redistributed). The transformation therefore becomes thermodynamically impossible once the austenite composition reaches the T_0' curve of the phase diagram. At this point, austenite and supersaturated bainitic ferrite of the same chemical composition have the same free energy. If, on the other hand, the bainite formed with its equilibrium composition, then the transformation could continue until the austenite achieves its equilibrium composition given by the usual $Ae3$ curve of the phase diagram, and the blocky regions of high carbon austenite would be consumed, giving a tough steel.

The fact that bainite growth is without diffusion causes large regions of austenite to remain untransformed, no matter how long the sample is held at the transformation temperature. The blocky regions of austenite can be eliminated by promoting further transformation to bainite, either by displacing the T_0' curve to larger carbon concentrations, or by reducing the average carbon concentration. The former can be accomplished by modifying the susbtitutional solute content of the steel (i.e., the phase stabilities).

Fig. 33b shows the impact transition curves of three steels, the first (Fe–0.4C–3Mn–2Si wt%) has large quantities of blocky austenite (Fig. 4a) and very poor impact toughness at room temperature. The nickel–containing steel has a T_0' curve which is at larger carbon concentrations (Fig. 33a); the Fe–0.2C–3Mn–2Si steel has half the carbon concentration of the bad steel. Both of these new steels have much better impact properties because the modifications allow more bainitic ferrite to form at the expense of blocky austenite[40, 41]. The better toughness is achieved without any sacrifice to strength.

15   Summary

The future looks good for carbide–free bainitic steels, which are now well understood both with respect to the atomic mechanism of transformation and the mechanical behaviour of its composite microstructures. One outstanding problem is a quantitative theory for the influence of elements such as silicon which inhibit

(a)
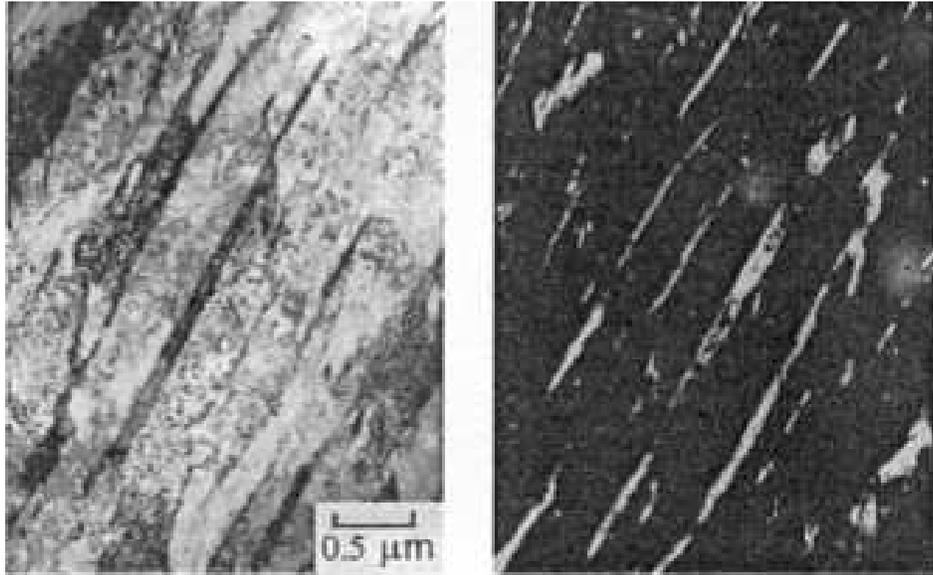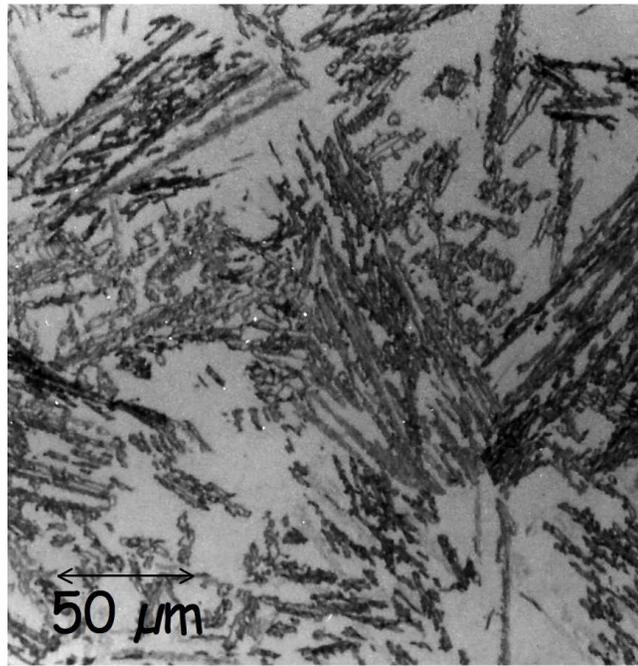
(b)

Figure 32: (a) Transmission electron micrograph of a mixture of bainitic ferrite and stable austenite. (b) Optical micrograph of upper bainite in an Fe–0.43C–3Mn–2.02Si wt% showing the blocks of retained austenite between sheaves of bainite.
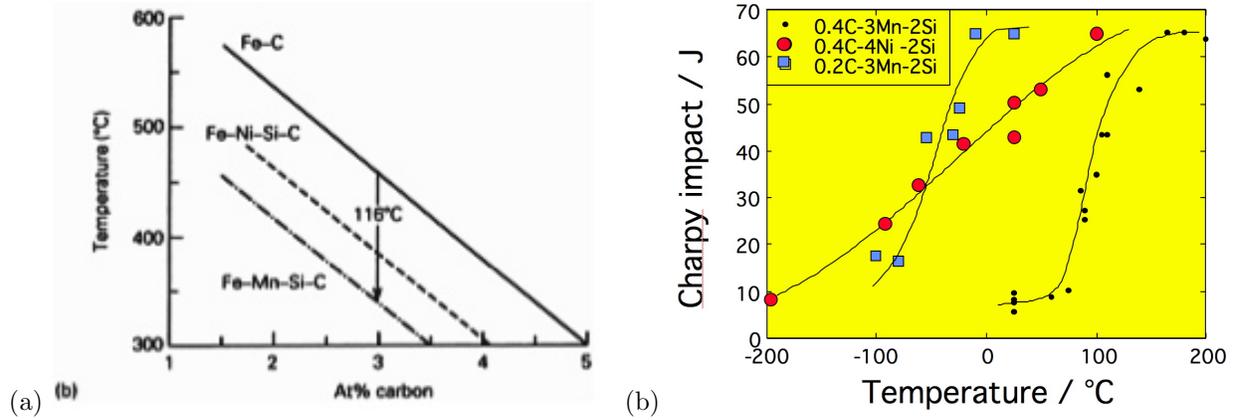
Figure 33: (a) Calculated T_0' curves for the Fe–C, Fe–Mn–Si–C and Fe–Ni–Si–C steels. (b) Experimentally determined impact transition curves showing how the toughness improves as the amount of blocky austenite is reduced. The chemical compositions stated are approximate.

cementite precipitation from austenite.

References

[1] E. Swallow and H. K. D. H. Bhadeshia. High resolution observations of displacements caused by bainitic transformation. *Materials Science and Technology*, 12:121–125, 1996.

[2] A. B. Greninger and A. R. Troiano. Kinetics of the austenite to martensite transformation in steel. *Trans. ASM*, 28:537, 1940.

[3] H. K. D. H. Bhadeshia and A. R. Waugh. Bainite: An atom probe study of the incomplete reaction phenomenon. *Acta Metallurgica*, 30:775–784, 1982.

[4] H. K. D. H. Bhadeshia. Rationalisation of shear transformations in steels. *Acta Metallurgica*, 29:1117–1130, 1981.

[5] H. K. D. H. Bhadeshia. *Bainite in Steels, 2nd edition*. Institute of Materials, London, 2001.

[6] A. Ali and H. K. D. H. Bhadeshia. Aspects of the nucleation of Widmanstätten ferrite. *Materials Science and Technology*, 6:781–784, 1990.

[7] H. K. D. H. Bhadeshia. Critical assessment: Diffusion–controlled growth of ferrite plates in plain carbon steels. *Materials Science and Technology*, 1:497–504, 1985.

[8] C. G. Mateo and H. K. D. H. Bhadeshia. Nucleation theory for high–carbon bainite. *Materials Science and Engineering A*, 378A:289–292, 2004.

[9] J. W. Christian. A theory for the transformation in pure cobalt. *Proceedings of the Royal Society of London A*, 206A:51–64, 1951.

[10] G. B. Olson and M. Cohen. A general mechanism of martensitic nucleation, parts i-iii. *Metallurgical Transactions A*, 7A:1897–1923, 1976.

[11] H. Conrad. Thermally activated deformation of metals. *Journal of Metals*, July:582–588, 1964.

[12] J. E. Dorn. Low temperature dislocation mechanisms. In A. R. Rosenfield, G. T. Hahn, A. L. Bement, and R. I. Jaffee, editors, *Dislocation dynamics*, page 27, New York, 1968. McGraw Hill.

[13] G. B. Olson, H. K. D. H. Bhadeshia, and M. Cohen. Coupled diffusional–displacive transformations. *Acta Metallurgica*, 37:381–389, 1989.

[14] R. F. Hehemann. The bainite transformation. In H. I. Aaronson and V. F. Zackay, editors, *Phase Transformations*, pages 397–432, 1970.

[15] K. C. Russell. Linked flux analysis of nucleation in condensed phases. *Acta Metallurgica*, 16:761–769, 1968.

[16] H. K. D. H. Bhadeshia. A thermodynamic analysis of isothermal transformation diagrams. *Metal Science*, 16:159–165, 1982.

[17] J. L. Lee and H. K. D. H. Bhadeshia. A methodology for the prediction of time-temperature-transformation diagrams. *Materials Science and Engineering A*, A171:223–230, 1993.

[18] University of Cambridge and NPL. Materials Algorithms Project, www.msm.cam.ac.uk/map/mapmain.html.

[19] M. Takahashi and H. K. D. H. Bhadeshia. A model for the microstructure of some advanced bainitic steels. *Materials Transactions JIM*, 32:689–696, 1991.

[20] H. Matsuda and H. K. D. H. Bhadeshia. Kinetics of the bainite transformations. *Proceedings of the Royal Society of London A*, A460:1710–1722, 2004.

[21] J. W. Christian. *Theory of Transformations in Metal and Alloys, Part I.* Pergamon Press, Oxford, U. K., 3 edition, 2003.

[22] F. G. Caballero and H. K. D. H. Bhadeshia. Very strong bainite. *Current Opinion in Solid State and Materials Science*, 8:186–193, 2005.

[23] M. Takahashi and H. K. D. H. Bhadeshia. Model for the transition from upper to lower bainite. *Materials Science and Technology*, 6:592–603, 1990.

[24] C. H. Young and H. K. D. H. Bhadeshia. Strength of mixtures of bainite and martensite. *Materials Science and Technology*, 10:209–214, 1990.

[25] Y. Tomita and K. Okabayashi. Mechanical properties of high strength steel of mixed microsturctures. *Metallurgical Transactions A*, 16A:73–82, 1985.

[26] A. A. Howe. Ultrafine grained steels: industrial prospects. *Materials Science and Technology*, 16:1264–1266, 2000.

[27] N. Tsuji, Y. Ito, Y. Saito, and Y. Minamino. Strength and ductility of ultrafine grained aluminium and iron produced by ARB and annealing. *Scripta Materialia*, 47:893–899, 2002.

[28] Y. Ivanisenko, I. MacLaren, R. Z. Valiev, and H. J. Fecht. First observation of a shear–induced bcc to fcc transformation in nanocrystalline ferrite. *Advanced Engineering Materials*, 7:1011–1014, 2005.

[29] F. G. Caballero, H. K. D. H. Bhadeshia, K. J. A. Mawella, D. G. Jones, and P. Brown. Very strong, low–temperature bainite. *Materials Science and Technology*, 18:279–284, 2002.

[30] H. K. D. H. Bhadeshia. Large chunks of very strong steel. *Materials Science and Technology*, 21:1293–1302, 2005.

[31] C. Garcia-Mateo, F. G. Caballero, and H. K. D. H. Bhadeshia. Low–temperature bainite. *Journal de Physique Colloque*, 112:285–288, 2003.

[32] C. Garcia-Mateo, F. G. Caballero, and H. K. D. H. Bhadeshia. Acceleration of low–temperature bainite. *ISIJ International*, 43:1821–1825, 2003.

[33] M. Peet, S. S. Babu, M. K. Miller, and H. K. D. H. Bhadeshia. Three–dimensional atom probe analysis of carbon distribution in low–temperature bainite. *Scripta Materialia*, 50:1277–1281, 2004.

[34] M. Peet, C. Garcia-Mateo, F. G. Caballero, and H. K. D. H. Bhadeshia. Tempering of a hard mixture of bainitic ferrite and austenite. *Materials Science and Technology*, 20:814–818, 2004.

[35] C. Mack. *Proceedings of the Cambridge Philosophical Society*, 52:286, 1956.

[36] C. Garcia-Mateo and F. G. Caballero. Role of retained austenite on tensile properties of steels with bainitic microstructures. *Materials Transactions*, 46:1839–1846, 2005.

[37] M. Sherif, C. Garcia-Mateo, T. Sourmail, and H. K. D. H. Bhadeshia. Stability of retained austenite in TRIP–assisted steels. *Materials Science and Technology*, 20:319–322, 2004.

[38] M. Y. Sherif. *Characterisation and development of nanostructured, ultrahigh strength, and ductile bainitic steels*. University of Cambridge, 2005.

[39] E. J. Garboczi, K. A. Snyder, J. F. Douglas, and M. F. Thorpe. Geometrical percolation threshold of overlapping ellipsoids. *Physical Review E*, 52:819–828, 1995.

[40] H. K. D. H. Bhadeshia and D. V. Edmonds. Bainite in silicon steels: a new composition property approach i. *Metal Science*, 17:411–419, 1983.

[41] H. K. D. H. Bhadeshia and D. V. Edmonds. Bainite in silicon steels: a new composition property approach ii. *Metal Science*, 17:420–425, 1983.

Further Reading

[1] Abe, F., Bainitic and martensitic creep-resistant steels, *Current Opinion in Solid State and Materials Science* **8**, 313, 2004.

[2] Bhadeshia, H. K. D. H., The lower bainite transformation and the significance of carbide precipitation, *Acta Metallurgica* **28**, 1103, 1980.

[3] Bhadeshia, H. K. D. H., The bainite transformation: unresolved issues, *Materials Science and Engineering* **A273–275**, 58, 1999.

[4] Bhadeshia, H. K. D. H., *Bainite in Steels*, 2nd edition, Institute of Materials, London, UK, 2001.

[5] Bhadeshia, H. K. D. H., 52nd Hatfield Memorial Lecture: Large chunks of strong steel, *Materials Science and Technology* **21**, 1293, 2005.

[6] Brown, P. M. and Baxter, D. P., Hyper-strength bainitic steels, *Proceedings of Materials Science and Technology 2004*, New Orleans, Louisiana, p. 433, 2004.

[7] Caballero, F. G. and Bhadeshia, H. K. D. H., Very strong bainite, *Current Opinion in Solid State and Materials Science* **8**, 251, 2004.

[8] Christian, J. W., *Theory of Transformations in Metals and Alloys*, 3rd edition, Pergamon Press, Oxford, 2003.

[9] Christian, J. W. and Edmonds, D. V., The bainite transformation, *Phase Transformations in Ferrous Alloys*, TMS-AIME, Pennsylvania, USA, p. 293, 1984.

[10] Garcia–Mateo, C., Caballero, F. G. and Bhadeshia, H. K. D. H., Development of hard bainite, *ISIJ International* **43**, 1238, 2003.

[11] Hehemann, R. F., The bainite reaction, *Phase Transformations*, American Society for Metals, Ohio, USA, p. 397, 1970.

[12] Pickering, F. B., *Physical Metallurgy and the Design of Steels*, Applied Science Publishers, London, UK, 1978.

[13] Takahashi, M., Kinetics of the bainite transformation, *Current Opinion in Solid State and Materials Science* **8**, 213, 2004.